wzu20461439080
@163.com

Effects of cold rolling and annealing treatment on microstructure and properties of CoFeNiMnV high-entropy alloys

Heyang Xin, Xizhang Chen, Yanhu Wang, Chuanchu Su, Dongqun Xin, Jiayi Xia, Yu Liang

College of Mechanical and Electrical Engineering, Wenzhou University, Wenzhou, 325035, China

Abstract: In this study, a combination of cold rolling (CR) and annealing treatment is used to investigate the evolution of the microstructure and mechanical properties of CoFeNiMnV high-entropy alloys (HEAs) fabricated by powder plasma arc additive manufacturing (PPA-AM). The deposited CoFeNiMnV HEAs exhibit a face-centered cubic (FCC) structure with a small amount of σ phase precipitation. After 50% cold rolling, the microstructure of CoFeNiMnV HEAs is severely deformed along the rolling direction, which the grain size is obviously refined, and the hardness and strength of the alloy are significantly improved (compared to the PPA-AM deposited sample, the hardness is about 1.9 times higher and the tensile strength is about 1.4 times higher). The rolled CoFeNiMnV HEAs is annealed at 500°C, 700°C and 900°C, respectively, for 60 min. The results show that annealing at 500°C has little effect on the microstructure and dislocation density of the alloy, and the alloy still maintains high strength and hardness. After annealing at 700°C and 900°C, with the increase of annealing temperature, the dislocation density of the alloy is significantly reduced, the σ phase is gradually dissolved, and the recrystallized grains and annealing twins are significantly coarsened, which makes the strength of the alloy decrease and the elongation increase significantly. CoFeNiMnV HEAs annealed at 700°C after cold rolling exhibit an excellent high strength-toughness combination.

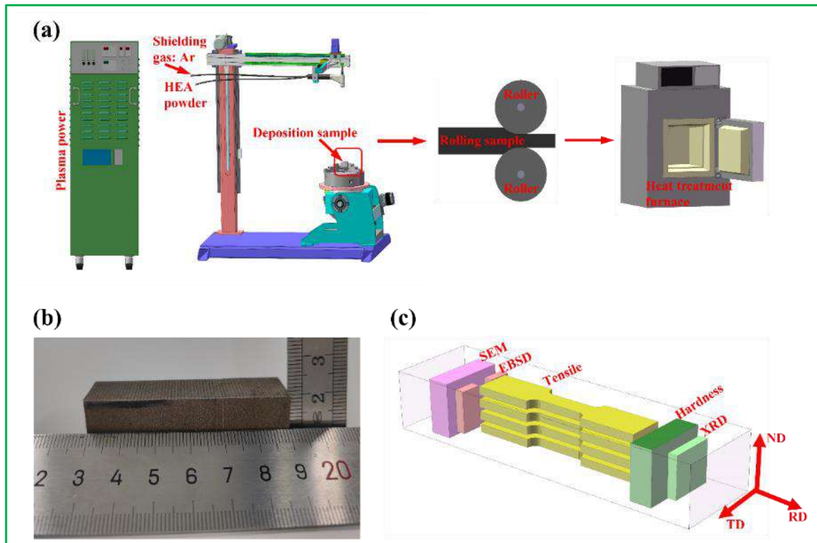

Fig.1 (a) Preparation of CoFeNiMnV HEAs by PPA-AM, and schematic diagram of cold rolling and annealing process; (b) Representative samples of CoFeNiMnV awaiting rolling (units mm) and (c) Sampling location diagram for microstructure observation and mechanical properties detection.

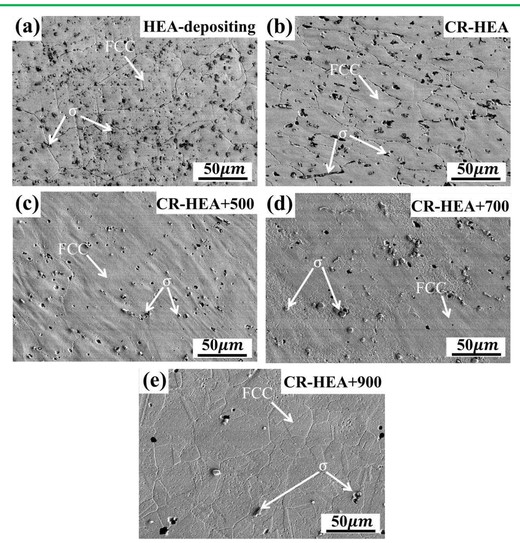

Fig.2 SEM images of PPA-AM deposited, cold rolled, and annealed samples：(a) HEA-depositing;(b) CR-HEA;(c) CR-HEA+500;(d) CR-HEA+700;(e) CR-HEA+900.

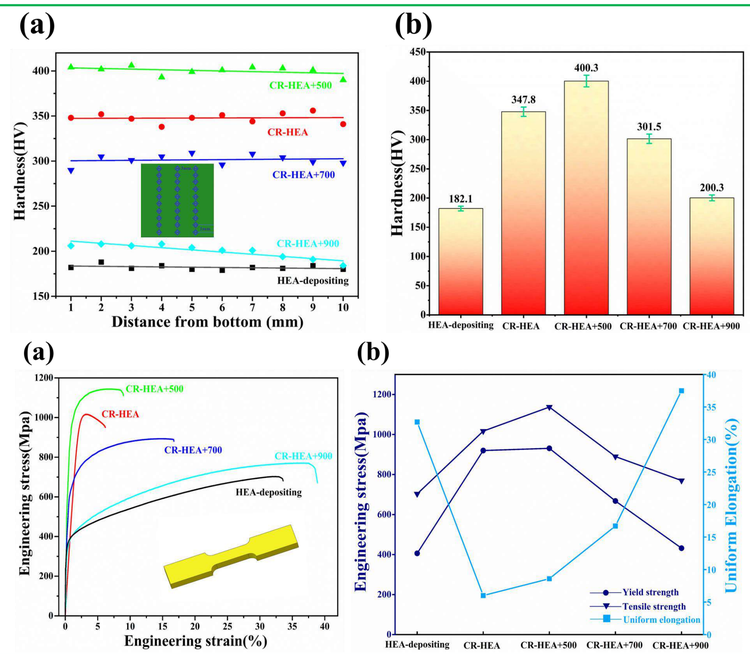

Fig.3 (a) Microhardness distribution values of PPA-AM deposited, cold rolled and annealed samples; (b) The average hardness of each treated sample.

Fig.4 Tensile properties of PPA-AM deposited, cold rolled and annealed samples: (a) engineering stress-strain curves; (b) changing tendency of yield strength, tensile strength and uniform elongation.

WZU20461439085
@163.com

Investigation on the microstructure and friction mechanism of novel CoCrCu0.2FeMox high-entropy alloy coating using plasma arc cladding

Jiayi Xia, Dongqun Xin, Xizhang Chen , Heyang Xin

College of Mechanical and Electrical Engineering, Wenzhou University, Wenzhou, 325035, China

Abstract: To explore the effect of the Mo element on the microstructure and frictional properties of the coating, we prepared novel CoCrCu0.2FeMox (ie., x values in molar ratio, where x=0.1, 0.2, 0.3) high-entropy alloy coatings on the surface of 304 stainless steel substrate by using plasma arc cladding technology in this work. By using scanning electron microscope, X-ray diffractometer, microhardness tester and three-dimensional laser measurement microscope, we analyzed the effect of Mo element on the phase structure, microscopic morphology, microhardness and friction properties of the coatings. The friction mechanism of the coatings was carefully investigated. The experimental results show that the CoCrCu0.2FeMox high-entropy alloy coatings are composed of Face-Centered Cubic phase (FCC phase) and δ phase (rich Mo, Cr). The microscopic morphology of the alloy changes gradually from branch crystal to eutectic structure with the increase of Mo content. At the same time, the hardness of the coatings increased, while the wear volume, wear rate and average surface roughness decreased. When the Mo content is increased to 0.3, the delamination of the oxide layer is effectively reduced. The friction mechanism changed from abrasive wear, oxidation wear and fatigue spalling to abrasive wear.

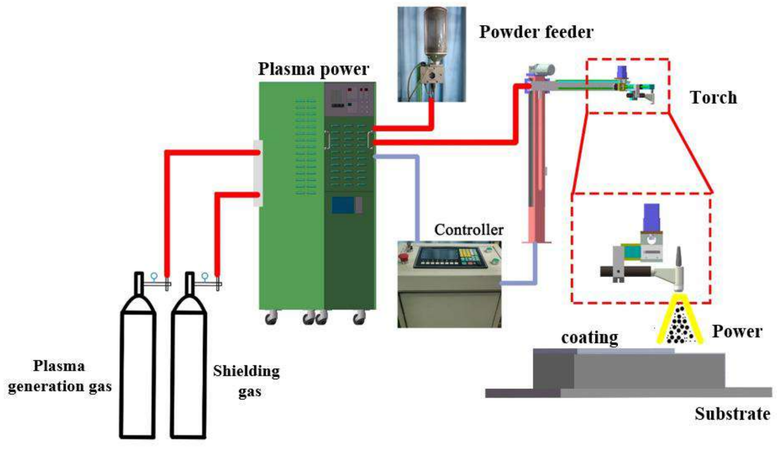

Fig.1 Preparation of CoCrCu0.2FeMox high-entropy alloy coating using plasma arc cladding

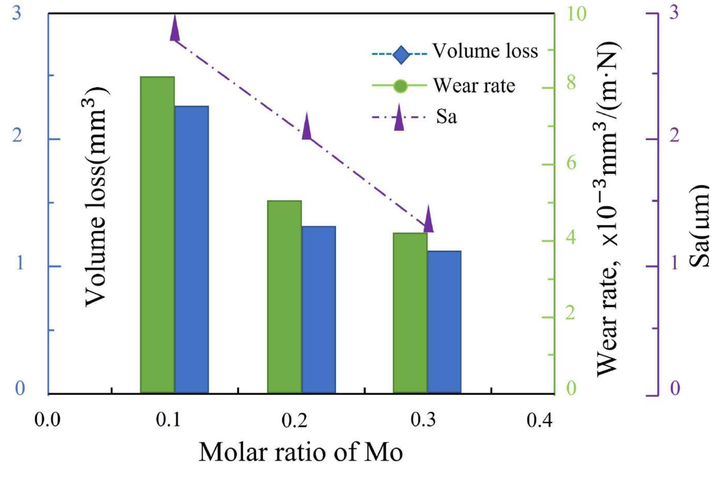

Fig.2 The cross-section profile of a typical wear trace

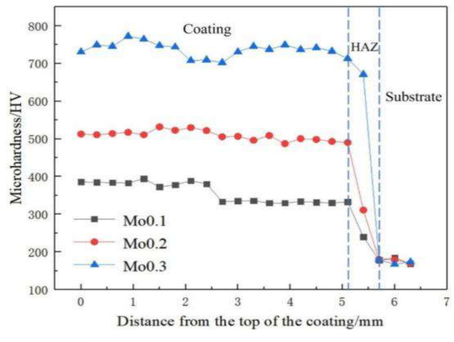

Fig. 3 Distribution of microhardness with depth on the cross section of Mox high-entroy alloy coating

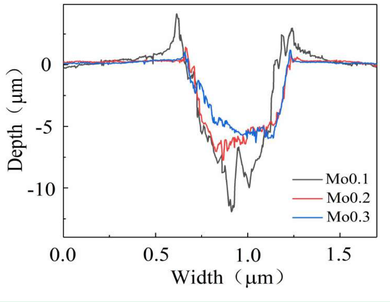

Fig.4 Typical cross-sectional profiles of the wear tracks for all three studied HEAs

IV International Conference and School "Advanced High Entropy Materials"
September 26-30, 2022

№4

abzalov396@mail.ru

Abzalov N.I., Lisina T.G., Seplyarskii B.S., Kochetkov R.A.

MACROKINETICS OF COMBUSTION OF GRANULAR MIXTURES (Ti+C)-Ni. EFFECT OF GRANULES SIZE

One of the methods for obtaining metal-ceramic powders for applying protective coatings is self-propagating high-temperature synthesis (SHS).

Scaling up the process of obtaining composite materials from a mixture of powders of metals and nonmetals by the SHS method requires reproducibility of combustion parameters and predictability of the properties of the resulting products. As shown in [1], in the synthesis of titanium carbide with a nickel binder, it is possible to achieve stabilization of the process and the phase composition of the products by using a mixture granulated with an alcohol solution of polyvinyl butyral (PVB). However, the influence of such important characteristics of mixtures as the size of granules on the combustion process has not been studied.

In the present work, for granular mixtures of (1)-90%(Ti+C)+10%Ni and (2)-80%(Ti+C)+20%Ni with a PVB content of about 1%, the combustion regularities were studied when the size of the granules changed.

Figure 1. Scheme of the experimental setup.

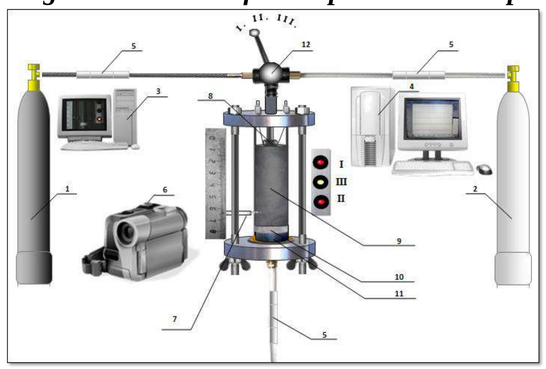

1 – nitrogen cylinder 2 – argon cylinder 3 – computer for recording video signal, 4 – computer for recording sensor readings via ADC, 5 – flow and pressure sensors, 6 – digital video camera, 7- tungsten-rhenium thermocouple 5/20, 8 – electric spiral 9 – charge, 10 – layer mineral wool, 11 – metal mesh, 12 – a three-position switch that allows you to change both the cylinder from which the gas is purged (position I – nitrogen; II – argon) and turn off the gas supply (position III) to the reaction chamber.

Table 1. Burning velocities of granules (100%)(Ti+C)+xNi of different fractions.

№	Fraction, mm	d, mm	(1) U, mm/s, x=10%	(2) U, mm/s, x=20%
1	0.4-0.8	0.6	51	34
2	0.8-1.2	1.0	64	37
3	1.4-2.0	1.7	78	43
4	0.6-1.6	1.1	63	40

Figure 2. Burning velocities of (100%-x)(Ti+C)+xNi granules of different fractions.

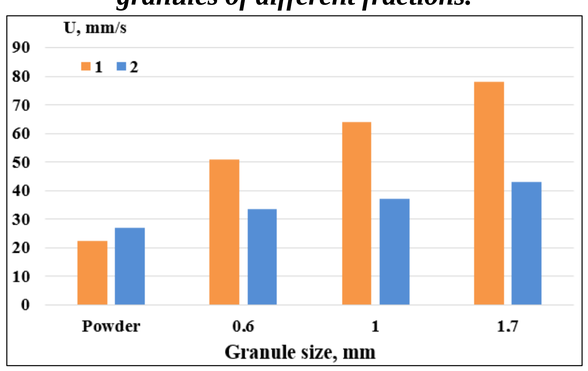

Figure 3. Photos of the charges from granules of fraction 1.7 mm and 0.6 mm of composition 80%(Ti+C)+20%Ni.

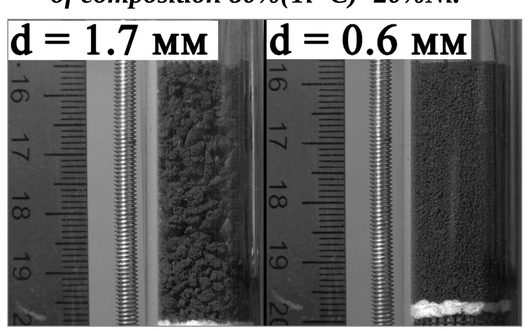

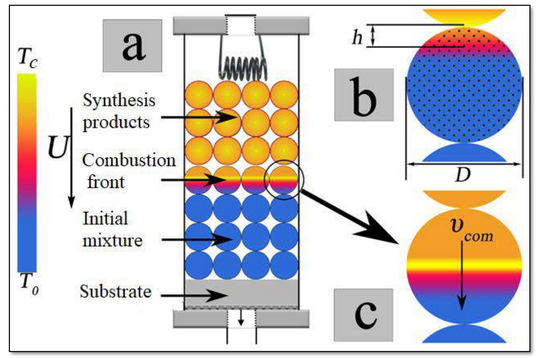

Figure 4. Schematic representation of the conductive combustion regime.

$$t = t_{com} + t_{ig} \quad (1)$$

$$t = d/U \quad (2)$$

$$h = (at)^{1/2} \quad (3)$$

$$U = v_{com}\, d / (d + v_{com}\, t_{ig}) \quad (4)$$

$$\begin{cases} U_1 = \dfrac{v_{com} * d_1}{(d_1 + v_{com} * t_{ig})} \\ U_2 = \dfrac{v_{com} * d_2}{(d_2 + v_{com} * t_{ig})} \end{cases}, \quad (5)$$

Using values of combustion velocities (U_1, U_2) for two fractions (d_1, d_2) of the mixture, from a system of two equations with two unknowns, it is possible to determine the desired values of the v_{com} (burning rate of the substance of the granules) and t_{ig} (burning transfer time from one granule to another).

Figure 5. Summary results.

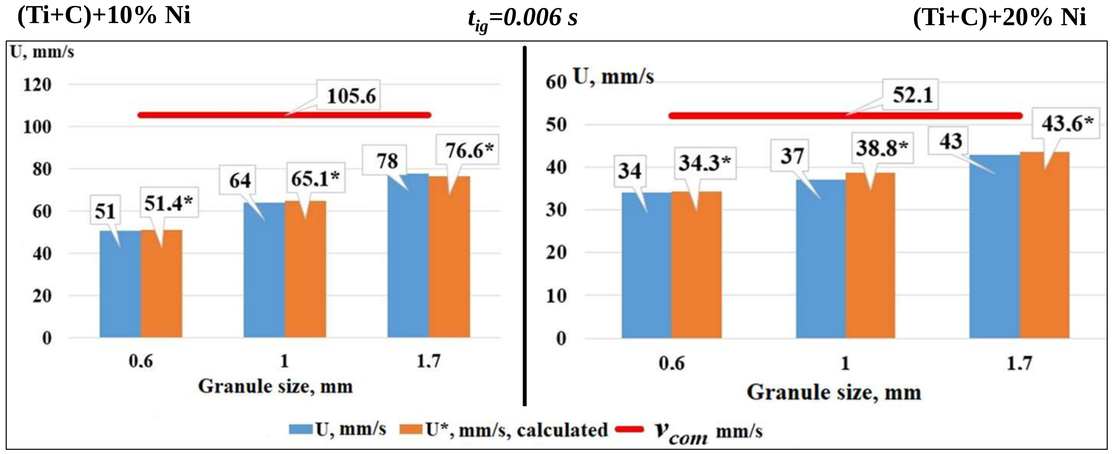

Conclusions: The combustion velocities of granular mixtures 10%(Ti+C)+90%Ni and 20%(Ti+C)+80%Ni, containing ~ 1% PVB, for fractions 0.4÷0.8; 0.8÷1.2; 1.4÷2 and 0.6÷1.6 mm turned out to be higher than for powder mixtures of the same composition.

Experimental data and calculations confirmed that for the combustion of all fractions of the studied mixtures the combustion velocity inside the granules and the time of combustion transfer between the granules do not depend on the size of the granules.

The combustion velocity of the granule substance was calculated and tuned out to be much higher than the velocity of burning of the powder mixture and the granular one.

The time of combustion transfer from granule to granule was determined and turned out to be the same for mixtures with 10% and 20% Ni and equal to 0.006 s.

References:

[1] B.S. Seplyarsky, R. A. Kochetkov, T. G. Lisina, N.I. Abzalov and M.A. Alymov. Phase composition and ... // Inorganic materials. – 2019. - Volume 55. - No. 11. - Ss. 1169-1175.

№5

azarov@bntu.by

THE CHARACTERISTICS OF POROUS MATERIALS FROM BASALT FIBERS

S.M. Azarau, E.E. Petyushik, A.A. Drobysh, T.E. Evtukhova
Minsk, Repablic of Belarus

In result of the conducted researches it is established that the sintering of basalt fiber at 1050 C and 1100°C forms a porous material with a structure characterized by a porosity of 52-75%, an average pore size of 8-18 μm, the permeability coefficient of (42-55) 10--12 m^2 , compressive strength 7-13 MPa. The results obtained prove that a porous material made of basalt fiber is capable of providing the specified characteristics when used as a basis for high-entropy materials.

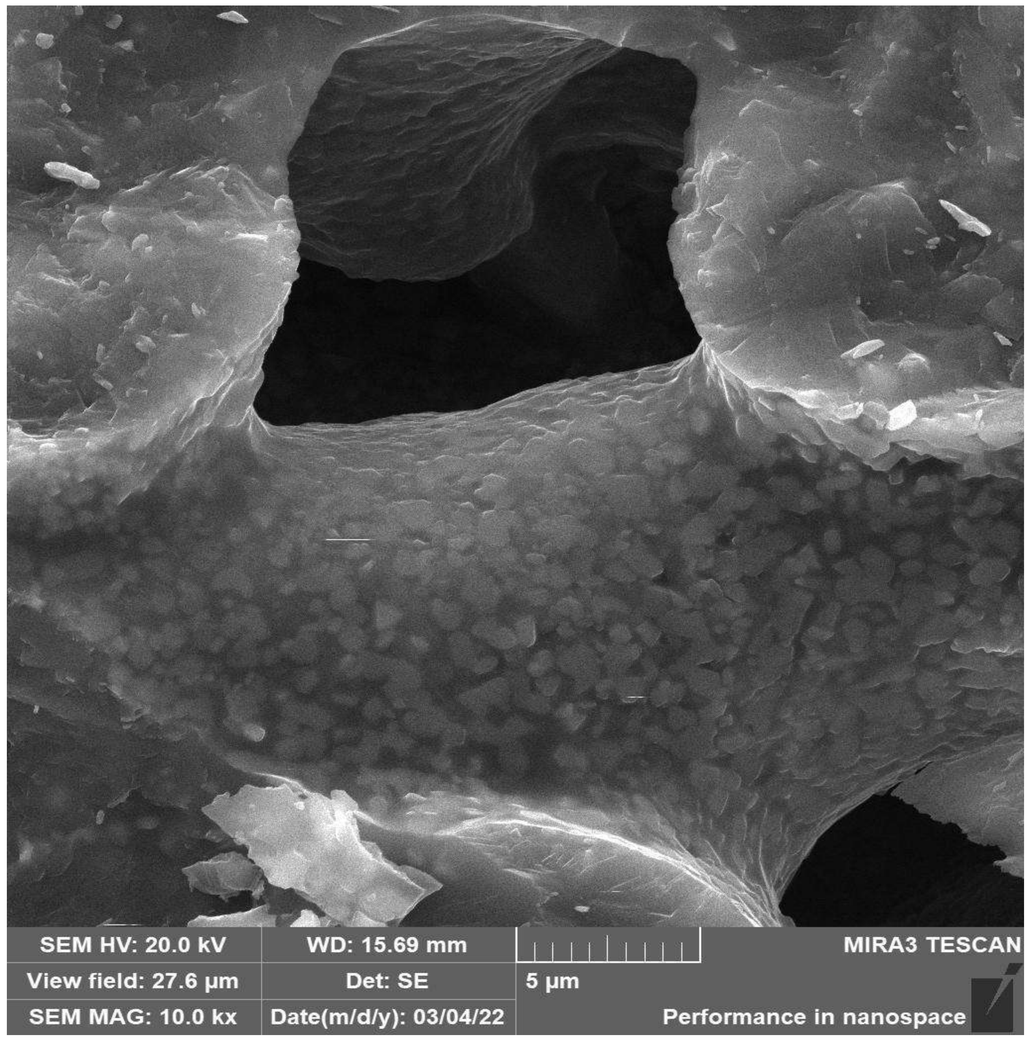

IV International Conference and School "Advanced High Entropy Materials"
September 26-30, 2022

№ 6

Tigj@yandex.ru

Merzhanov Institute of Structural Macrokinetics and Materials Science

Akopdzhanyan T.G., Rupasov S.I.

CHEMICALLY ACTIVATED COMBUSTION SYNTHESIS OF ALON UNDER HIGH NITROGEN PRESSURE

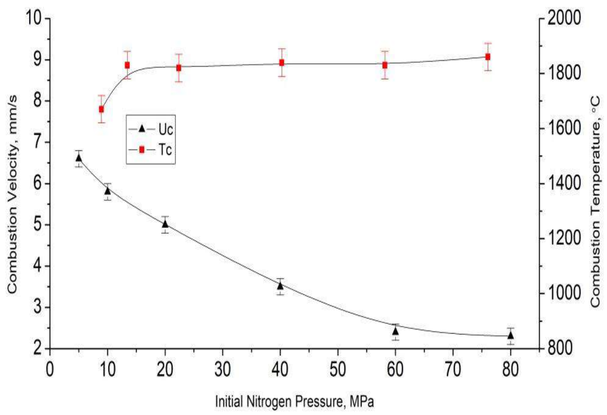

Figure 1. Dependence of the combustion temperature and velocity on starting nitrogen pressure.

This work explores the synthesis of aluminum oxynitride (AlON) by combustion of Al/Al2O3 mixtures under a high-pressure nitrogen atmosphere. To increase the exothermicity of combustion, we coupled Al oxidation and nitriding. Extra Al and $Mg(ClO_4)_2$ were introduced into the stoichiometric Al/Al2O3 mixture. $Mg(ClO_4)_2$ plays a dual role – the source of oxygen for Al oxidation and the source of Cl, which chemically activates the combustion and enhances gas-phase transport of reagents in the combustion front.

Figure 1 presents the dependence of the combustion temperature Tc and combustion front propagation velocity Uc on starting nitrogen pressure.
At 5 MPa the Tc is about 1650 °C. This value is considerably below the calculated adiabatic combustion temperature Tad (2070 °C). This difference is related to the hindered filtration of nitrogen into the combustion front due to the sub-optimal pore geometry of the pressed green body of the reactive mixture. Notably, the highest Uc was achieved at low pressures of nitrogen, suggesting that the main combustion-governing reaction was the oxidation of aluminum by magnesium perchlorate rather than nitridation of aluminum by gaseous N2. Additionally, the high pressure of nitrogen prevents the release of the gaseous admixtures from the combustion front, which in turn inhibits the spread of aluminum melt in the front and therefore reduces the combustion front propagation velocity.

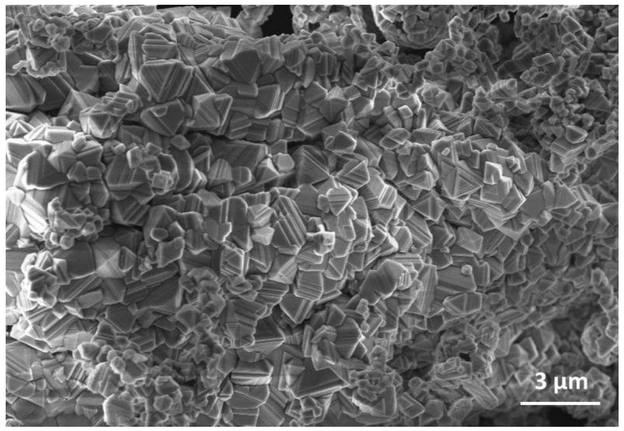

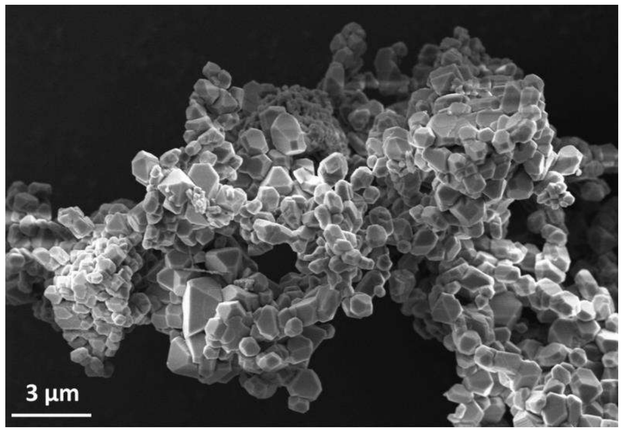

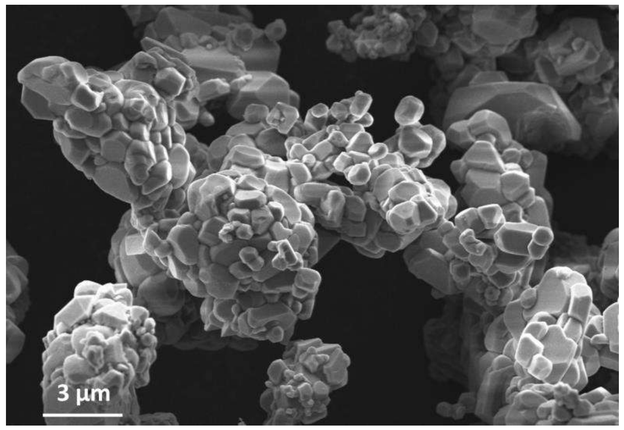

Figure 4. SEM images of AlON powder obtained with the addition of 0% (a), 0.5 wt. % (b) and 1 wt. % (c) of Y_2O_3 to the green reactive mixture.

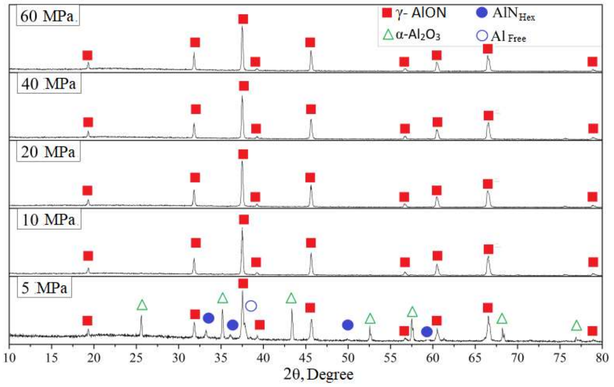

Figure 2. XRD of combustion products obtained at different starting nitrogen pressure.

The XRD analysis Figure 2 of combustion products reveals the presence of unreacted Al, AlN, and Al_2O_3 peaks and thus confirms that the lack of reactivity and incomplete nitridation at P_{N2}=5MPa prevents the formation of single-phase AlON. At pressures P≥10 MPa complete conversion is achieved, resulting in phase-pure AlON products. No phases were found which could be attributed to the $Mg(ClO_4)_2$ decomposition products.
Chemical analysis revealed the presence of 0.3 wt. % Mg and 0.5 wt. % Cl in the as-synthesized combustion products. This result suggests that the chlorine does not just evaporate from the combustion products, but instead participates in the phase formation processes and forms chlorides by-products. These by-products are advantageous during combustion but must be eliminated before sintering to minimize the pollution of the produced ceramics. Luckily, chlorides are water-solvable, so boiling the combustion products in distilled water for 30 minutes reduced the impurity content to 0.06 wt. % Mg and 0.04 wt. % Cl. Since the content of both Mg and Cl decrease 5-10 times, we conjecture that nearly all Mg was present in the form of water-soluble MgCl2 instead of magnesia or spinel.

Despite very similar combustion temperatures, combustion products obtained at PN2=10..60 MPa differed both in nitrogen content and in lattice constants of the AlON phase (Figure 3). An increase of PN2 resulted in a monotonous increase in both the AlON lattice parameter (from 7.948 up to 7.952 Å) and nitrogen content (from 3.4 to 4.1 %).

The combustion products obtained from mixture were characterized by a narrow particle size distribution (Figure 4a), which is usually optimal for structural ceramics. Since yttria additives are often used to improve the sinterability and optical properties of AlON ceramics, in this work we investigated the influence of introducing 0.5 and 1 wt. % of Y_2O_3 in the reactive mixture on the morphology of combustion products (Figure 4b, 4c). In comparison with the control sample (0% Y_2O_3, Figure 4a), the addition of 0.5 wt.% of Y_2O_3 (Figure 4 b) resulted in smoothing of the grains surface, which likely will enhance the structural refinement of combustion products during the milling. However, the increase of Y_2O_3 additive content to 1 wt. % induced a more pronounced sintering and agglomeration of the particles in the combustion products, which is counter-productive for the manufacturing of transparent ceramics.

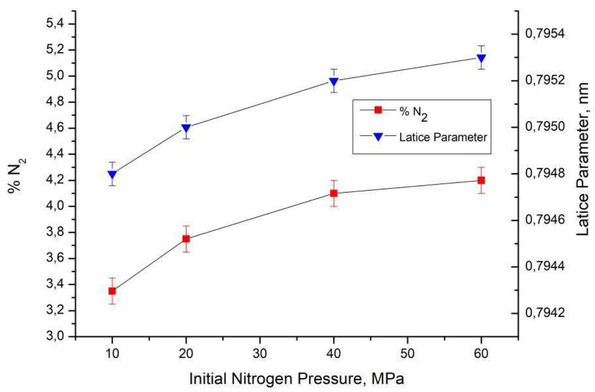

Figure 3. The dependence of nitrogen content and AlON lattice parameter on the P_{N2}

The as-synthesized AlON powders were characterized by 1-2 µm grains size. We added 0.5 wt. % of Y_2O_3 and mixture of Y_2O_3, MgO and La_2O_3 to the combustion products before synthesis (added to reactive mixture) and before ball milling (after synthesis). After ball milling, doped AlON powders were characterized by a surface area of 21.06 ± 0.0783 m^2/g and an average particle size of 1.5 µm. These powders were uniaxially pressed under 50 MPa load to produce cylindrical compacts, which were subsequently sintered at 1930 °C in a graphite furnace under 0.1 MPa nitrogen pressure for 10 h.
The sintered AlON samples were ground and polished, and their light transmittance (Figure 5) and mechanical properties were tested. One can see that the light transmittance of sintered samples improved with addition of Y_2O_3, MgO and La_2O_3 rather then Y_2O_3 and reaches up to 52%. The samples was characterized by hardness H=17.7±2.0 GPa, Young's modulus E=320±29 GPa, elastic recovery of 62,8%. This level of mechanical properties corresponds exactly to the commercial aluminum oxynitride (H= 17.65 GPa, E=334 GPa).

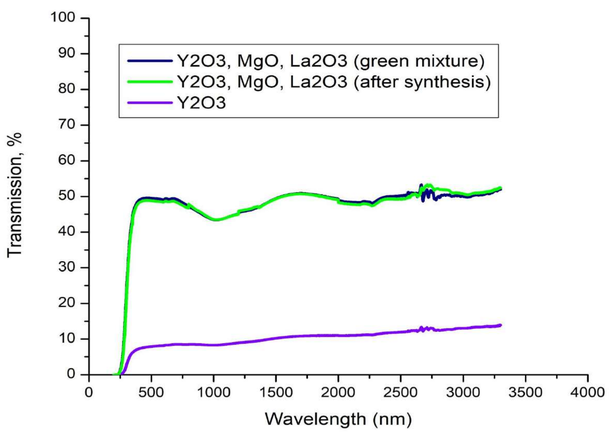

Figure 5. The image of AlON transparent samples (a) and their light transmittance (b).

IV International Conference and School "Advanced High Entropy Materials" September 26-30, 2022

№ 8

PHASE COMPOSITION AND MECHANICAL PROPERTIES OF NITROGEN-CONTAINING HIGH-ENTROPY ALLOYS

denis.0612@mail.ru

[1]Astapov D. O., [2]Reunova K. A., [1]Gurtova D. Yu., [2]Astafurova E. G.

[1]National Research Tomsk State University, [2]Institute of Strength Physics and Materials Science SB RAS

Introduction

The Cantor alloy has relatively low strength properties (YS~200 MPa at 297 K), but it is assumed that the formation of interstitial solid solutions, for example, by alloying with nitrogen atoms, and modification of the microstructure caused by solid-solution hardening help to obtain alloys with a significant increase in strength without significant loss of plasticity.

Materials and methods

The mechanical properties in 20Fe-20Mn-20Cr-20Ni-20Co (at. %, 0N-HEA), 20Fe-20Mn-20Cr-20Ni-19.2Co-0.8N (0.8N-HEA), 20Fe-20Mn-20Cr-20Ni-18.6Co-1.4N (1.4N-HEA) and 20Fe-20Mn-20Cr-20Ni-18.4Co-1.6N (1.6N-HEA) alloys have been investigated. The cast billets were subjected to a thermal-mechanical treatment which consisted of annealing at 1200°C for 2 hours, cold rolling with a 80 % reduction and annealing at 1200°C for 2 hours with a final water-quenching. All HEAs have been investigated using the X-ray diffraction analysis (XRD), light, transmission and scanning electron microscopy, tensile testing at temperatures 77 K and 297 K.

Fig. 1 XRD patterns of the HEAs

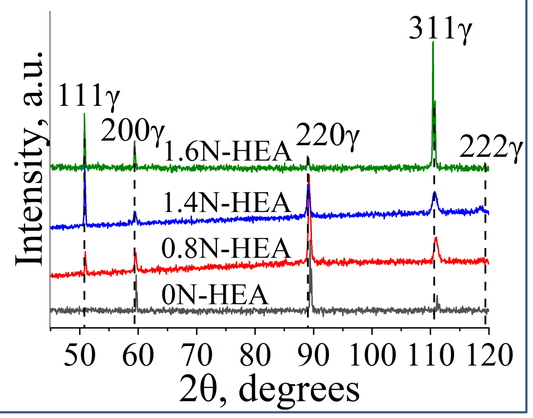

Notation	YS, MPa (77 K/297 K)	UTS, MPa (77 K/297 K)	El, % (77 K/297 K)	*a*, Å
0N-HEA	390/192	1825/877	92/61	3.598
0.8N-HEA	513/250	2044/1026	61/61	3.604
1.4N-HEA	632/288	1930/1209	49/67	3.607
1.6N-HEA	560/375	970/1413	9/69	3.608

Table 1. Tensile properties and the lattice parameter of austenitic phase *(a)* in alloys: YS – the yield strength, UTS – the ultimate tensile stress, El – elongation to failure.

Experimental results

All alloys possess single-phase austenitic structure with FCC crystal lattice. Interstitial nitrogen causes a distortion of a crystal lattice and increases a lattice parameter of austenite (Fig. 1, Table 1). Nitrogen-alloying increases the YS and UTS of Cantor alloy, and these values are dependent on nitrogen concentration (Table 1). The elongation values in nitrogen-alloyed alloys in low-temperature deformation regime are much lower than that in 0N-HEA. However, at 297 K nitrogen-alloying weakly influences this value (Table 1).

SEM images of fracture surfaces of HEAs specimens at the temperature 77 K

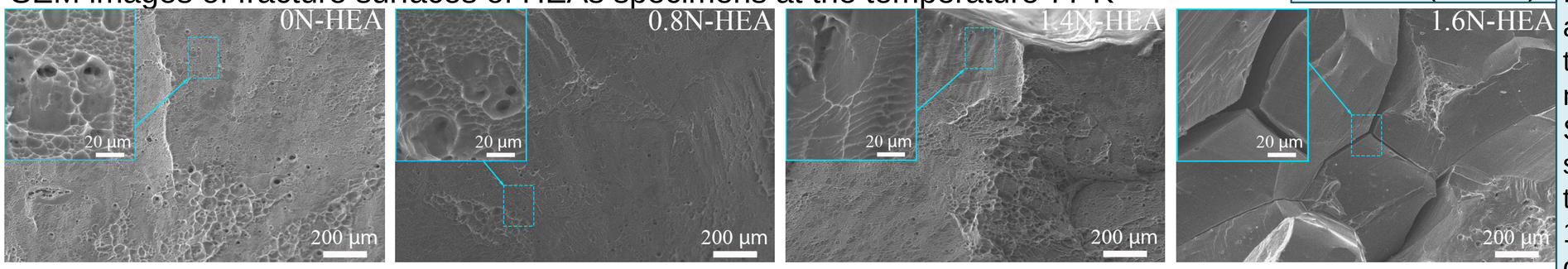

SEM images of fracture surfaces of HEAs specimens at the temperature 297 K

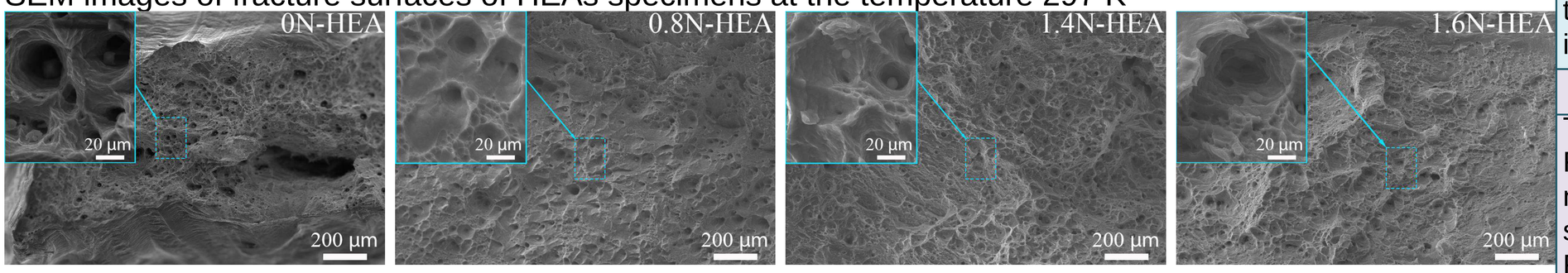

In high-temperature deformation regimes, all alloys are characterized by ductile transgranular fracture. At 77 K, the numerous shallow dimples are seen in SEM images of the Cantor fracture surfaces. Similar dimple-like morphology is typical of 0.8N-HEA and 1.4N-HEA. For 1.6N-HEA, the brittle intergranular cracking dominates but the rare fragments of transgranular dimple fracture are also seen in fracture surfaces.

Conclusion

The results demonstrate that doping of FeMnCrNiCo high-entropy alloy with nitrogen atoms promotes the formation of a single-phase solid solution based on the FCC crystal structure and improves the strength characteristics of the initial alloy.

The research was supported by the Russian Science Foundation (project No. 20-19-00261).

IV International Conference and School "Advanced High Entropy Materials"
September 26-30, 2022

№9

THE EFFECT OF SEVERE PLASTIC DEFORMATION ON STRUCTURE AND PROPERTIES OF MEDIUM ENTROPY ALLOYS WITH TWIP/TRIP EFFECTS

Astakhov I. I., Povolyaeva E. A., Shaysultanov D. G., Stepanov N. D. and Zherebtsov S. V.
Laboratory of Bulk Nanostructured Materials, Belgorod State University, 85 Pobeda Str., 308015, Belgorod, Russian Federation
1257502@bsu.edu.ru

Abstract

In this work, medium-entropy iron-rich alloys obtained by vacuum-arc melting were used as program materials. The alloys were rolled to 80% at room temperature and then annealed at 900°C for 10 minutes with further water cooling. In the recrystallized state, the alloys were subjected to high-pressure torsion at room temperature on Bridgman anvils at a speed of 0.5 rpm. The anvil rotation angles were 180° (N0.5), 360° (N1), and 1080° (N3) at a pressure of 6.5 GPa.

The study of the initial recrystallized structure showed that the alloys have a two–phase structure consisting of the FCC matrix and «islands» of the martensitic BCC phase. Particles of the $M_{23}C_6$ carbides were found inside the grains and along boundaries. The HPT treatment leads to the formation of an inhomogeneous, strongly deformed microstructure with (sub) grains of ~ 50 nm after 0.5 revolutions (180°). The samples after three revolutions (N3) showed the maximum values of microhardness; in addition, attractive mechanical properties of the alloys were revealed during tensile tests at room and cryogenic temperatures. The relationship between the HPT parameters, structure and mechanical properties of alloys is discussed..

Microstructure Evolution during HPT

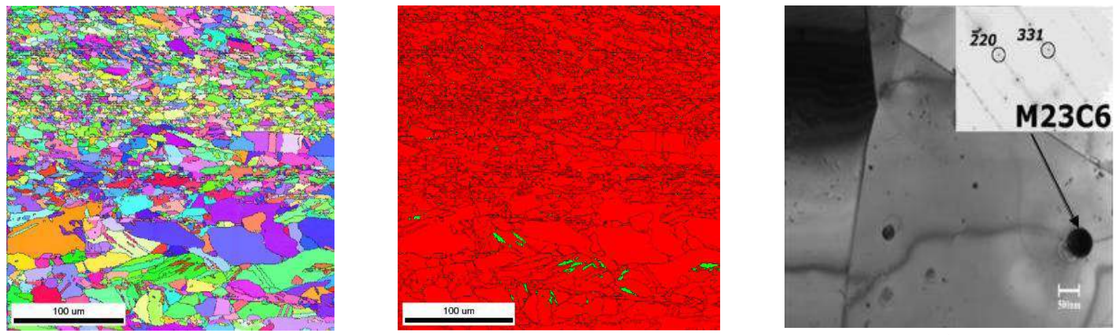

a) **b)** **c)**

Fig.1-SEM image of the microstructure of $Fe_{60}(CoNi)_{30}Cr_{9.5}C_{0.5}$ alloy (a) orientation distribution map; (b) phase map. TEM image of $Fe_{60}(CoNi)_{30}Cr_{9.5}C_{0.5}$(c) alloy.

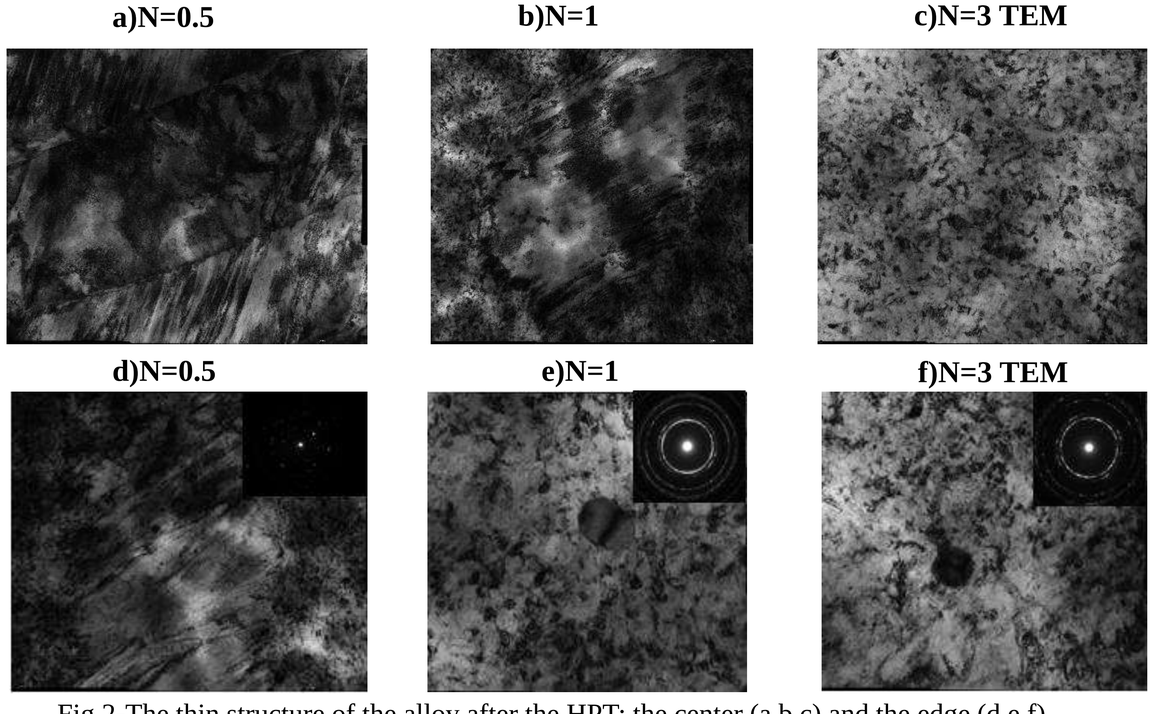

Fig.2-The thin structure of the alloy after the HPT: the center (a,b,c) and the edge (d,e,f).

Mechanical Properties after HPT

Table 1 - Mechanical properties of samples after HPT

Condition	$\sigma_{0,2}$, МПа	$\sigma_в$, МПа	δ, %
CR80%+Ann 900°C 10min	354	911	49
HPT	1560	1770	31

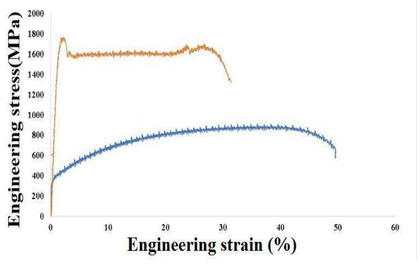

Fig.3-Stress-strain curves of $Fe_{60}(CoNi)_{30}Cr_{9.5}C_{0.5}$ alloy in the initial state (a) and after the HPT.

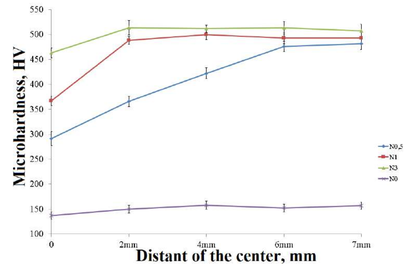

Fig.4-Distribution of microhardness from the center to the edge for the initial state and samples processed by the HPT method

Conclusions

The study showed that the $Fe_{60}(CoNi)_{30}Cr_{9.5}C_{0.5}$ alloy in its initial state has a recrystallized two-phase structure consisting of FCC and BCC phases, with a volume fraction of 93% and 4%, respectively. The average size of recrystallized grains was 12.7±4.6μm. Particles of carbides of the $M_{23}C_6$ type with a volume fraction of 3% and an average size of 60 nm were found inside the grains and along its boundaries. Processing by the HPT method at room temperature leads to the formation of an inhomogeneous, strongly deformed microstructure with (sub) grains of ~ 50 nm after turning 180°. The evolution of the microstructure was associated with intense twinning caused by deformation, and the development of the substructure led to a gradual grinding of the microstructure. It is shown that the ultimate strength of the alloy strongly depends on the deformation by the HPT method. Thus, the tensile strength of sample N3 increased from 911 MPa to 1170 MPa, compared with the initial state, with a decrease in plasticity from 49% to 31%.

Financial support from the Russian Science Foundation (Grant No. № 20-79-10093) is gratefully acknowledged. The work was carried out using the equipment of the Joint Research Center of Belgorod State National Research University «Technology and Materials» with financial support from the Ministry of Science and Higher Education of the Russian Federation within the framework of agreement No. № 075-15-2021-690 (unique identifier for the project RF----2296.61321X0030).

IV International Conference and School "Advanced High Entropy Materials" September 26-30, 2022

STRUCTURES AND MECHANICAL CHARACTERISTICS OF LAYERED COMPOSITE MATERIAL BASED ON TIB/TIAL/TI

frau.london2013@yandex.ru

Bazhina A.D., Konstantinov A.S., Chizhikov A.P., Bazhin P.M., Stolin A.M.

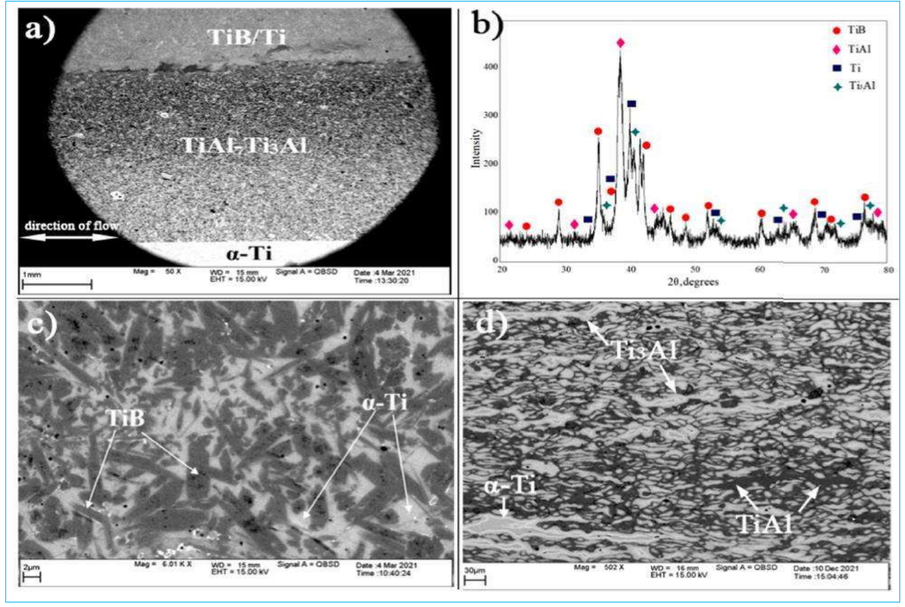

Fig. 1. (a) Macrostructure of the layered material, (b) X-ray powder diffraction pattern of the cross-section of the material, (c) microstructure of the upper region (Ti–B), (d) microstructure of the central region (Ti–Al).

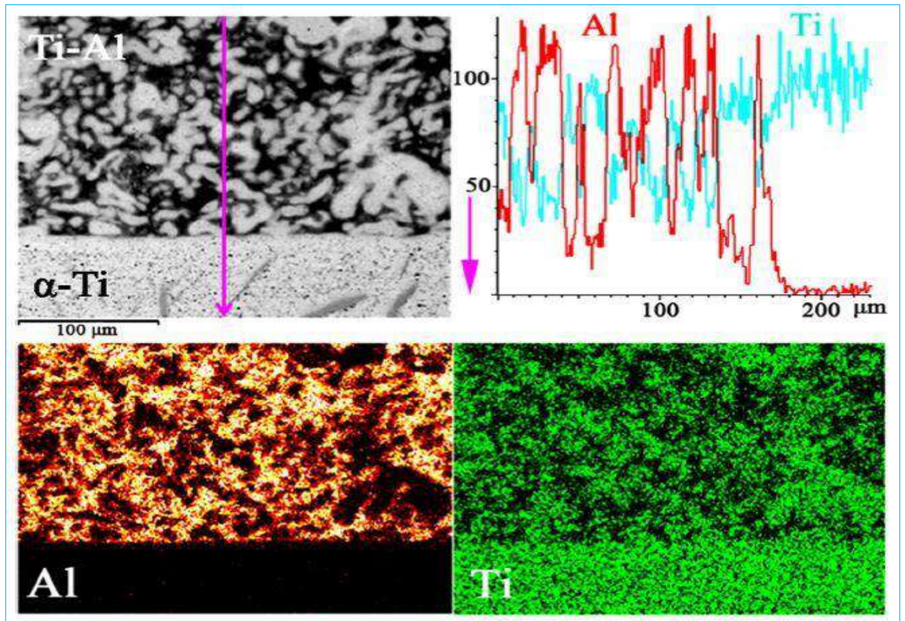

Fig. 2. Structure of the Ti–Al/α-Ti transition region.

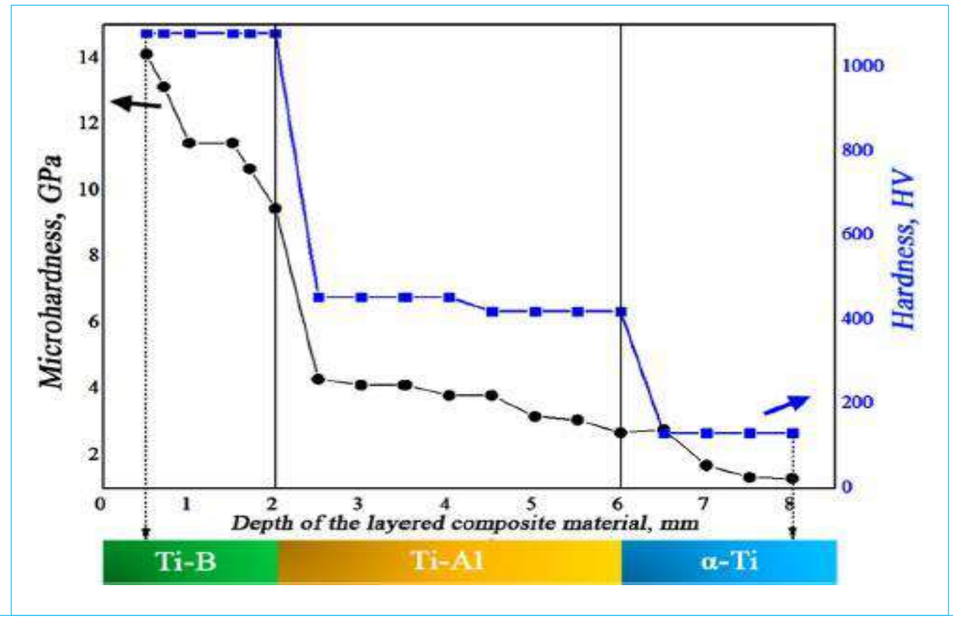

Fig. 3. Change in microhardness and hardness along the depth of the layered composite material.

Conclusions

(1) It has been found that, as a result of combustion and subsequent high-temperature shear deformation realized under conditions of unrestricted SHS compression, the orientation of intermetallic phases TiAl and TiAl along the direction of the material flow is observed. The orientation of intermetallic phases TiAl and TiAl in the intermetallic layer has a significant effect on the mechanism of crack propagation and makes it possible to reduce three times the stress intensity factor.

(2)The formation of diffusion boundaries between the composite ceramic (TiB/Ti) and intermetallic (TiAl, TiAl) layers proceeds according to the liquid/solid-phase mechanism, which makes it possible to increase the adhesive strength of these layers. The size of the interdiffusion zone depends on the choice of the composition of the initial reagents (as a consequence of the combustion temperature of the selected composition) and ranges from 40 to 450 μm.

(3)The absence of cracks in the ceramic layer of the composite is due to the presence of the hardening phase of titanium monoboride in the structure, which effectively prevents the propagation of cracks and strengthens the grain boundaries.

IV International Conference and School "Advanced High Entropy Materials"
September 26-30, 2022

№ 11

E-mail: tbarinova@ism.ac.ru

SELF-PROPAGATING HIGH-TEMPERATURE SYNTHESIS (SHS) TECHNOLOGY FOR DISPOSAL OF RADIOACTIVE WASTE

T. V. Barinova, V.Yu. Barinov, I.D. Kovalev, A.S. Shchukin, V.N.Semenova

Merzhanov Institute of Structural Macrokinetics and Materials Science, Russian Academy of Science, Chernogolovka, 142432 Russia

The aim: Immobilization of radioactive waste (RW) into mineral-like matrices

(*Model experiments*)

1.Immobilization of the entire spectrum of RW – Sr, Cs, actinides, rare earths, and corrosion products. Mineral-like matrices based on: $CaTiO_3$ + $CaZrTi_2O_7$ + $CsAlSi_2O_6$ + alloy FeCrNi .

2. Immobilization of the actinides / Zr / rare earth group. Mineral-like matrices based on $Y_2(Ti_{1-x}Zr_x)_2O_7$ ($x \leq 0,3$) + alloy FeCrNi .

3.Immobilization of ^{14}C graphite + fuel spillage (actinides, Cs, Sr). Mineral-like matrices based on TiC/Al_2O_3 + alloy FeCrNi. For fuel spillage immobilization: $CaTiO_3$ + $Y_3Al_5O_{12}$ + $(Ca,Ce)(Al,Ti)_{12}O_{19}$ + $Cs_2Ti_6O_{13}$.

4. Forced SHS compaction of large-sized (1750 g) matrices blocks in steel container:

Porosity (open) ≤ 3 %
Density 3,85-4,23 g/cm^3
Compression resistance 250 MPa
R^*_n, g/cm^2 · day:
Sr 0,5·10^{-6} – 0,7·10^{-7} (standard < 1·10^{-6});
Cs 5 ·10^{-6} – 1,5· 10^{-7} (standard < 1·10^{-5});
Re 10^{-7} – 10^{-8} (standard < 1·10^{-7}).
R^*_n – Leah rate (water resistance of ceramics**)**

IV International Conference and School "Advanced High Entropy Materials"
September 26-30, 2022

№ 13

Borisov S.I.
borisov.sg99@gmail.com

THE EFFECT OF PRIOR AUSTENITE GRAIN SIZE ON MICROSTRUCTURE AND TENSILE PROPERTIES OF TEMPERED LOW ALLOYED 0.2C STEEL

The preferred microstructure of recent developed advanced high-strength steels (AHSS) contain significant fraction of lath martensite. The initial austenitic structure has a significant effect on the dispersion of the elements of the quenched and tempered martensite. The mechanical properties of these steels are correlated with the size of the units of formed martensite.

Investigated steel: Fe-0.25%C-1.6%Si-1.47%Mn-0.51%Cr-0.27%Mo

The steel was subjected to homogenization annealing at a temperature of 1150°C. The steel was quenched from 900°C and tempered at 200°C; 280°C; 400°C; 500°C for 1 hour.

The deformation of the steel in the austenitic region is an effective way to refine the austenitic structure, which results in a decrease of the size of the elements of the martensitic structure after subsequent quenching.

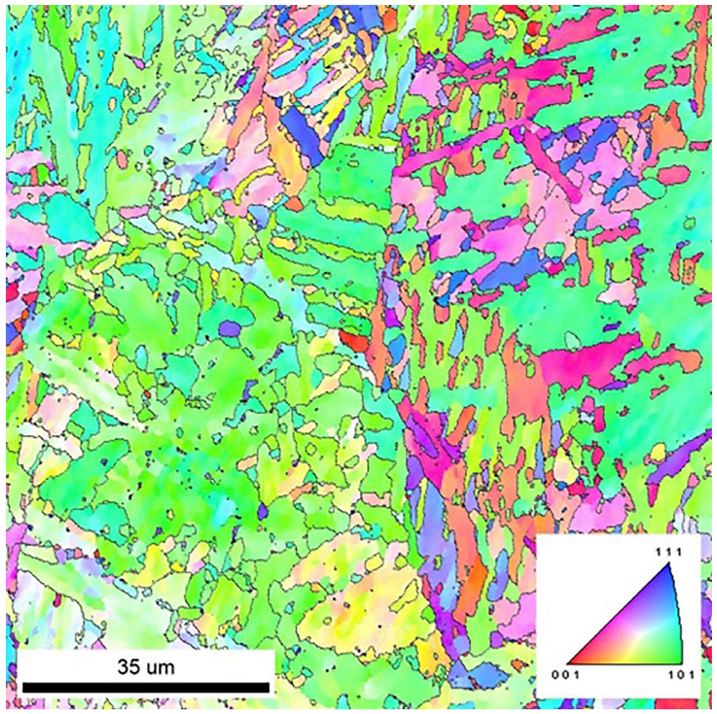

After pre-rolling

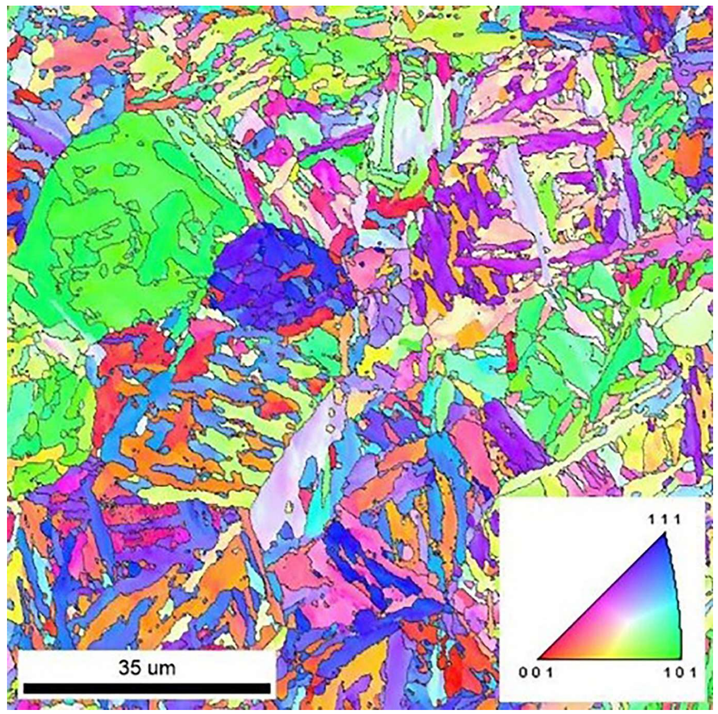

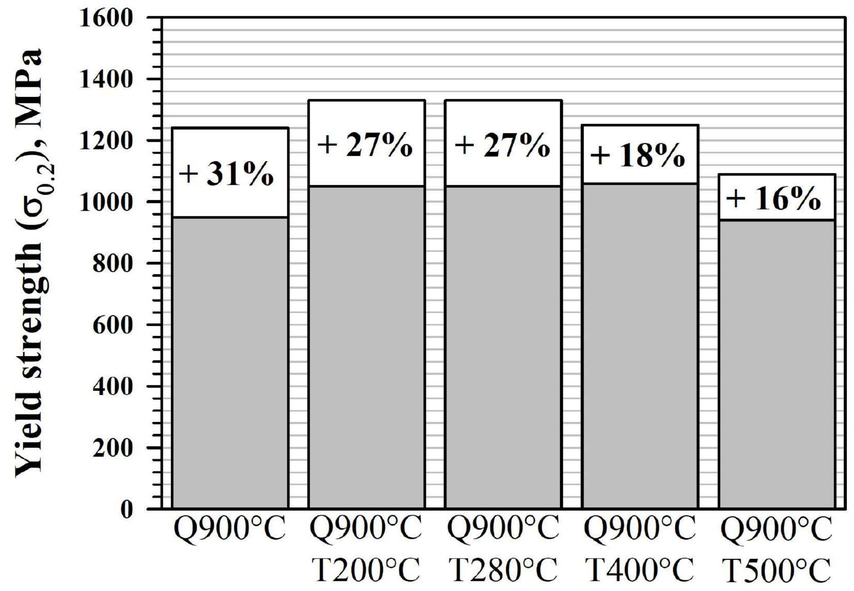

The investigation of the quenched steel structures in the initial state and after hot rolling operation showed that the average size of the PAGs was 32.7 μm and decreased to 16.6 μm in the pre-rolled steel.

The results of tensile tests showed that decrease in the PAG size by ~2 times leads to a significant increase in the yield and tensile strength. The maximum increase in tensile strength of +28% was observed in the quenched steel. The ductility of the steel with a smaller average size of the initial austenitic structure insignificantly decreases, by 1–2% on average.

Thus, the use of pre-rolling for high-strength low-alloy steels makes it possible to reduce the size of the PAGs and significantly increase the strength characteristics without a pronounced decrease in ductility.

IV International Conference and School "Advanced High Entropy Materials"
September 26-30, 2022

№ 14

DEEP OXIDATION OF CO AND PROPANE ON Co-CATALYSTS PRODUCED BY LOW-TEMPERATURE COMBUSTION ON MODIFIED SUPPORTS

inna2019@ismail.ac.ru

Bystrova I.M., Khomenko N.Yu., Borshch V.N.

Merzhanov Institute of Structural Macrokinetics and Materials Science of RAS, Chernogolovka, Russia

The support (silica gel) was modified with aluminum oxide by impregnation with a mixture of solutions of aluminum nitrate (oxidant) and urea (fuel), drying, and heating in an inert until combustion was initiated. A number of samples were subjected to calcination at temperatures of 500, 600 and 700°C. On the original and calcined samples by the same method was applied cobalt-containing active phase with a calculated content of 10% wt. cobalt in terms of metal.

Composition of catalyst samples

Образец	Расчетный состав
I	10% масс. Co /(10% масс. Al_2O_3 /силикагель, исходный)
II	10% масс. Co /(10% масс. Al_2O_3 /силикагель, прокаленный при 500°C)
III	10% масс. Co /(10% масс. Al_2O_3 /силикагель, прокаленный при 600°C)
IV	10% масс. Co /(10% масс. Al_2O_3 /силикагель, прокаленный при 700°C)
V	10% масс. Co /(20% масс. Al_2O_3 /силикагель, исходный)
VI	10% масс. Co /(20% масс. Al_2O_3 /силикагель, прокаленный при 500°C)
VII	10% масс. Co /(20% масс. Al_2O_3 /силикагель, прокаленный при 600°C)
VIII	10% масс. Co /(20% масс. Al_2O_3 /силикагель, прокаленный при 700°C)

Thermograms of the process of catalyst synthesis (range= 300°C) on a support containing 10% wt. Al_2O_3 : 1 – I, 2 – II, 3 – III, 4 – IV.

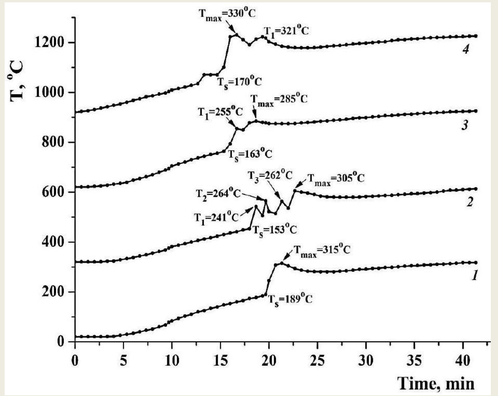

Phase composition of catalyst samples according to XRD data

Образец	Фазовый состав
I	$CoAl_2O_{4\ cub}$, $Co_2SiO_{4\ cub}$
II	$Al_{0.27}Co_{0.73}(Al_{0.73}Co_{1.27})O_{4\ cub}$
III	$Al_{0.27}Co_{0.73}(Al_{0.73}Co_{1.27})O_{4\ cub}$
IV	$Co_3O_{4\ cub}$, $Co_6Al_2O_{11\ cub}$
V	$Co_3O_{4\ cub}$, $CoAl_2O_{4\ cub}$
VI	$CoAl_2O_{4\ cub}$, $Co_2SiO_{4\ cub}$
VII	$CoAl_2O_{4\ cub}$, $Co_2SiO_{4\ cub}$
VIII	$Co_3O_{4\ cub}$, $CoAl_2O_{4\ cub}$

Specific surfaces of catalyst samples

Образец	Удельная поверхность, $м^2/г$
I	70,2
II	70,4
III	60,3
IV	76,8
V	62,3
VI	48,8
VII	53,7
VIII	63,1

Surface morphology of the catalyst sample (I) according to SEM data

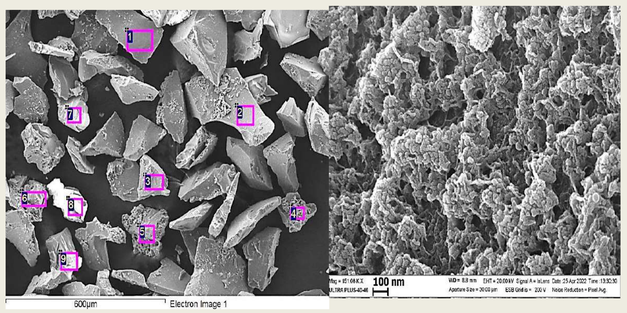

Surface morphology of the catalyst sample (V) according to SEM data

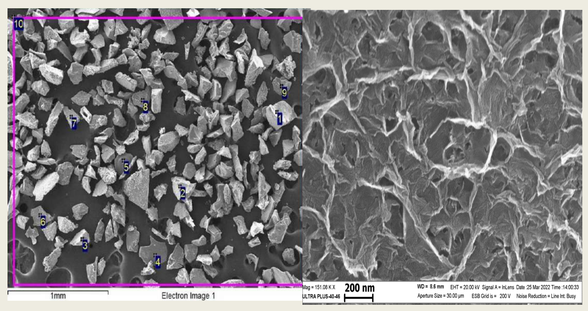

Surface morphology of the catalyst sample (VIII) according to SEM data

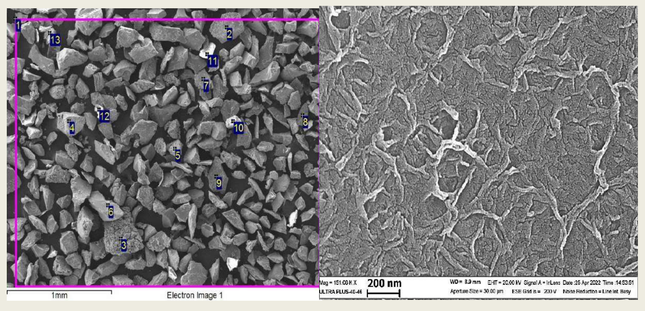

CO conversions vs. temperature over the catalysts: 1 – I, 2 – II, 3 – III и 4 – IV

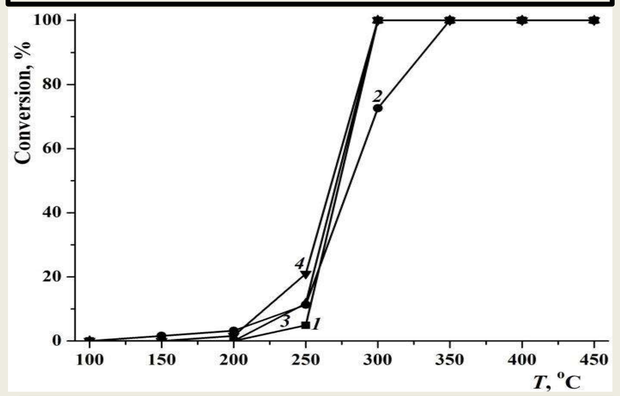

Elemental composition (% wt.) of the catalyst surface (I)

№ точки	O	Al	Si	Co
1	53.51	1.74	35.20	9.55
2	59.98	1.87	28.88	9.27
3	67.57	3.94	17.34	11.15
4	64.34	3.55	16.80	15.31
5	66.57	2.56	21.20	9.67
6	49.57	2.09	18.58	29.76
7	63.87	1.80	26.35	7.98
8	66.29	1.76	37.35	4.60
9	67.23	1.34	23.69	7.74

Elemental composition (% wt.) of the catalyst surface(V)

№ точки	O	Al	Si	Co
1	49.66	12.48	4.33	33.53
2	47.45	2.61	7.09	42.85
3	60.83	19.75	3.20	16.22
4	62.08	2.79	27.18	7.95
5	64.29	2.36	28.52	4.83
6	70.73	3.74	20.21	5.32
7	52.98	3.84	5.54	37.64
8	57.63	12.96	17.07	12.34
9	67.76	2.46	20.62	9.16
10	81.77	2.38	8.19	7.66

Elemental composition (% wt.) of the catalyst surface(VIII)

№ точки	O	Al	Si	Co
1	71.76	3.66	11.80	12.78
2	46.01	9.44	2.75	41.80
3	9.72	2.59	1.21	86.48
4	28.08	2.92	4.84	64.16
5	44.20	5.26	11.53	39.01
6	45.47	4.62	8.13	41.78
7	53.26	4.77	27.91	14.06
8	39.40	2.90	41.82	15.88
9	69.15	2.92	25.01	2.92
10	58.13	6.14	8.55	27.18
11	38.94	3.90	7.98	49.18
12	75.42	2.74	18.06	3.78
13	71.17	3.10	21.56	4.17

Propane conversions vs. temperature over the catalysts: 1 – I, 2 – II, 3 – III и 4 – IV.

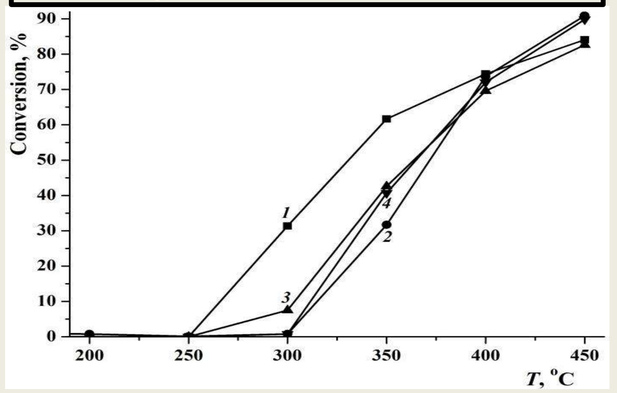

IV International Conference and School "Advanced High Entropy Materials"
September 26-30, 2022

№ 16

THE REASON FOR THE INCREASE IN COMBUSTION RATE OF THE POWDER MIXTURE TI+C DILUTED WITH COPPER

Vasilyev D.S., Seplyarskii B.S., Kochetkov R.A., Lisina T.G.

E-mail:
d.s.vasilyev@mail.ru

The purpose of this work is to explain the nature of the increase in the front velocity with a decrease in the combustion temperature, detected when diluting powder mixtures with Ti+C copper, and to propose a quantitative measure to determine the effect of impurity gas release on the combustion rate of powder mixtures using the **convective-conductive combustion model (CCM).**

Materials and methods of experiments

In the work we used: poly-disperse Ti powder of various fractions; poly-disperse Cu powder; carbon black; 4% solution of polyvinylbutyral in ethyl alcohol (for granulation).

The stoichiometry of the initial mixtures was calculated for the following main reactions:

Ti + C → TiC

Ti + C + 20 wt.% Cu → TiC + 20 wt.% Cu

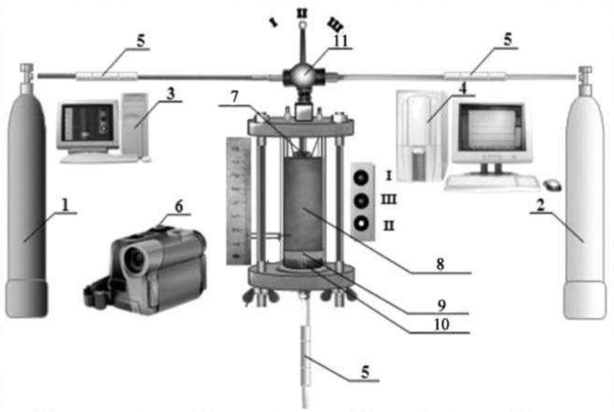

Fig. 1. Experimental installation

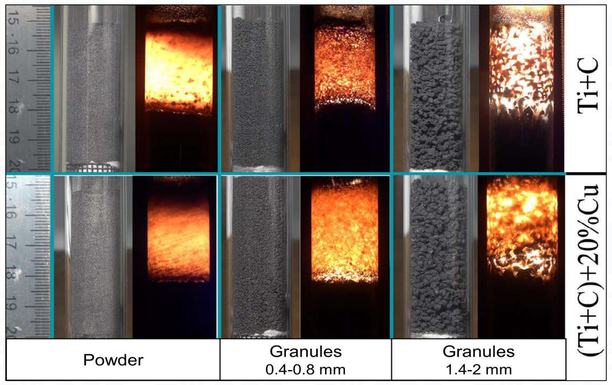

Fig. 2. Photographs of the powder and granular mixtures Ti + C and Ti+C +20%Cu during combustion

The results contradict the theoretical dependences on the combustion temperature for powder mixtures: **a decrease in the combustion temperature should lead to a decrease in the combustion rate!**

To explain the results obtained, we use CCM.

$$d < L,\ L = a_c/u_p \quad (1)$$

$$t_h < t,\ t_h = d^2/4a \text{ and } t = L/u_p = a_c/U_p^2 \quad (2)$$

$$h < D \quad (3)$$

$$h = (a_c\, t_{ig})^{1/2} \quad (4)$$

$$t_{ig} \le t_b = D/u \quad (5)$$

$$t_b = t_{com} + t_{ig} \quad (6)$$

$$u = u_{com} / (1 + u_{com}\, t_{ig}/D) \quad (7)$$

	Ti+C			(Ti+C)+20%Cu		
d, μm	u_{com}, mm/s	t_{ig}, c	u_{com}/U_p	u_{com}, mm/s	t_{ig}, s	u_{com}/u_p
31.5	90	0.007	7.5	71	0.006	5.3
77	46	0.017	5.8	44.5	0.013	3.6
107	33	0.019	4.7	33	0.015	2.8
142	24	0.023	4.8	24.5	0.016	2.3

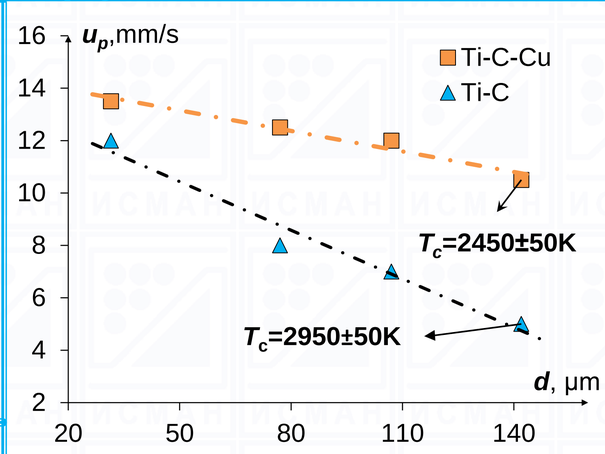

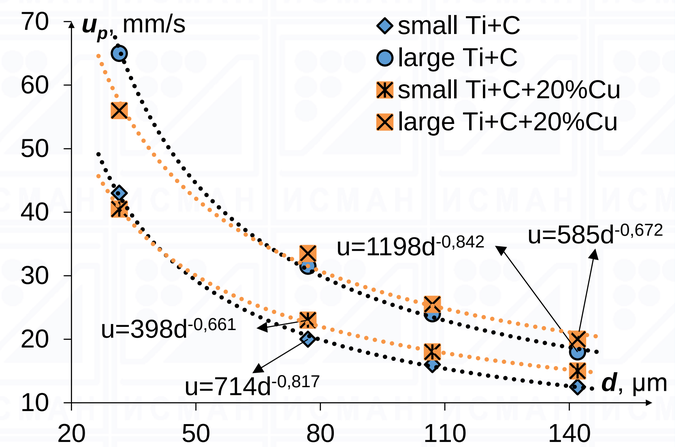

Fig. 3. Combustion rates of powder and granular mixtures of Ti+C and Ti+C+20%Cu depending on the particle size of Ti

Table 1. Results of calculation of heating conditions *(1)*, *(2)* for metal particles Me=Ti, Cu in powder mixtures.

d(Me), μm		u_p, mm/s	*L*, μm	t_h (Me), ms		*t*, ms		Heat	
Ti+C (T_{ad}=3300 K; T_c=2950±50 K)									
31.5		12	83	0.031		7		+	
77		8	125	0.183		6		+	
107		7	143	0.361		20		+	
142		5	200	0.635		40		+	
Ti+C+20%Cu (T_{ad}=2550 K; T_c=2450±50 K)									
Ti	Cu			Ti	Cu	Ti	Cu	Ti	Cu
31.5	40	13.5	74	0.031	0.027	5	5	+	+
77		12.5	80	0.183		6	5	±	+
107		12	83	0.361		7	7	-	+
142		10.5	95	0.635		9	9	-	+

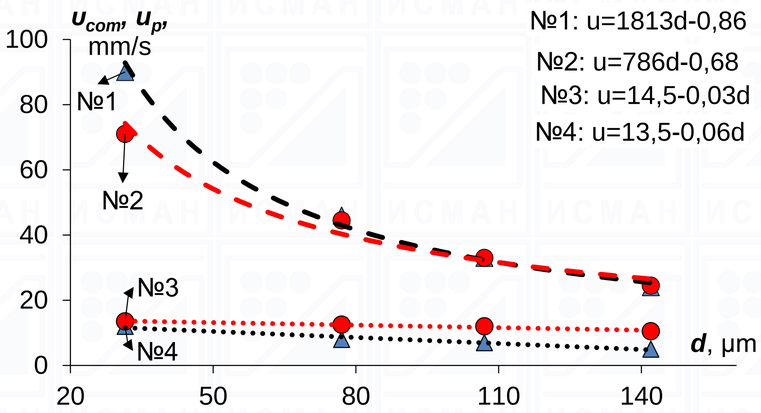

Fig. 4.The dependence of the combustion rate of the substance of the granules u_{com} (1,2) and the combustion rate and powder mixtures u_p (3,4) of the compositions Ti+C (1,4) and Ti+C+20%Cu (2,3) on the characteristic size *d* of titanium particles.

IV International Conference and School "Advanced High Entropy Materials"
September 26-30, 2022

№17

1196573@bsu.edu.ru

PREDICTION OF ELONGATION TO FRACTURE OF HIGH-ENTROPY ALLOYS USING NEURAL NETWORK

Vereshchak M.V., Klimenko D.N., Stepanov N.D., Zherebtsov S.V.

Laboratory of Bulk Nanostructured Materials, Belgorod State University, 85 Pobeda Str., 308015, Belgorod, Russian Federation.

Abstract

High entropy alloys (HEAs), sometimes also called multi-principle element alloys, were originally discovered by Yeh and Cantor. In contrast to traditional alloys, which are based on one principal element, HEAs were defined as alloys with five or more principal elements in equal or near-equal atomic percentages (5-35 at.%). The machine learning approaches (especially artificial neural network (ANN)) are promising methods for designing new high-entropy alloys with optimal properties [4]. In the present work the ANN approach was used for prediction of compressive ductility of high-entropy alloys at room temperature.

Neural network architecture

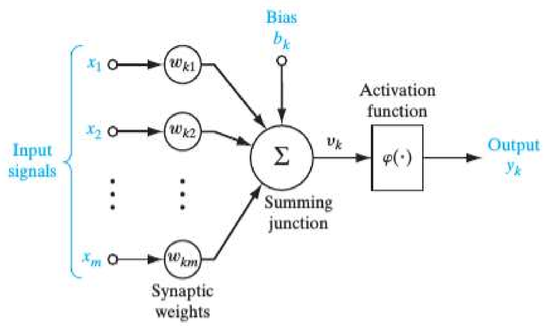

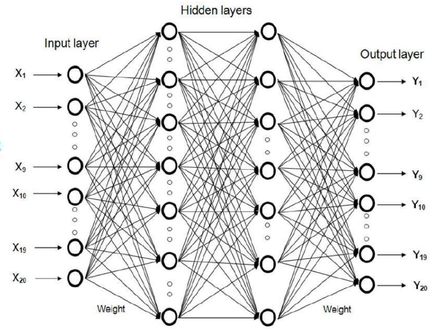

Optimal selection of features

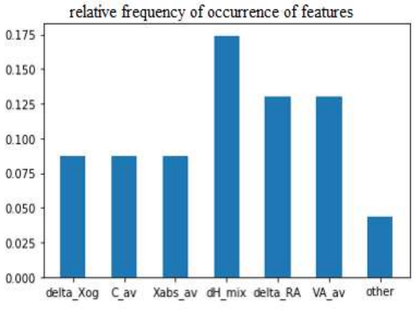

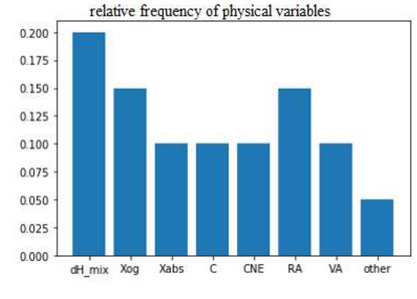

The main factor potentially affecting the accuracy of a machine learning model is the set of features used. To do this, it is important to create a set of descriptors that best describe the plasticity behavior of alloys.

On previous stage, the sets of features for some machine learning algorithms were selected by genetic algorithm. A statistical analysis of the selected features was carried out. The result of the analysis were histograms for the relative frequency of physical quantities and features. The most frequent features were used as descriptors for training the artificial neural network.

From the histograms obtained, it can be concluded that the optimal set of features is a set of the following parameters:

$\delta\chi_{og}$, $\bar{C}$, δRA , ΔH_{mix} , $\overline{VA}$, $\overline{\chi_{abs}}$, $\overline{CNE}$

Results

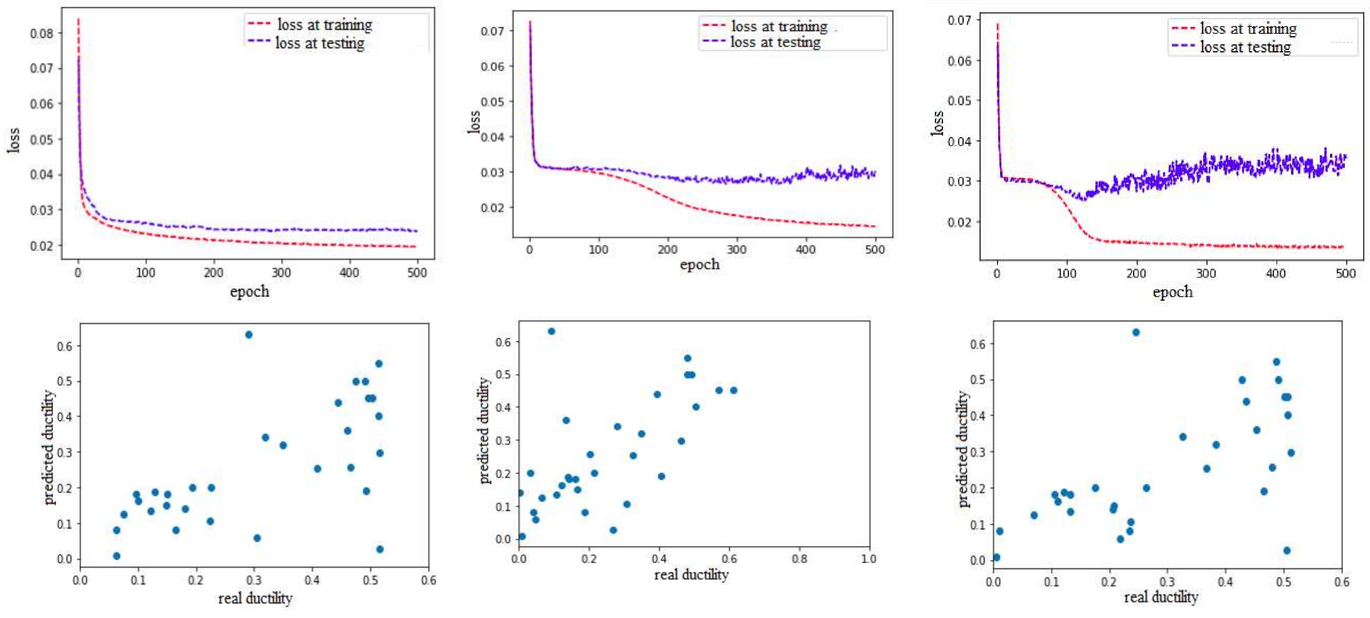

For determination of optimal ANN configuration, we calculated accuracy for a set of ANNs with the different number of hidden layers (from 1 to 3) and neurons (from 10 to 30). The ReLU function was used as an activation function for hidden layers, and the output function was a sigmoid.

The predictions on the test set of alloys are shown in the figures. A two-layer neural network with 14 neurons in each hidden layer best predicts the plasticity value for high-entropy alloys.

N	10	12	14	16	18	20	22	24	26	28	30
error	0.07	0.057	0.08	0.05	0.074	0.072	0.065	0.072	0.076	0.1	0.06

N	10	14	18	22	28
2 hidden layers	0.057	0.043	0.05	0.062	0.058
3 hidden layers	0.044	0.08	0.07	0.065	0.06

Acknowledgements

The authors gratefully acknowledge the financial support from the Russian Science Foundation Grant no. 19-79-30066 (https://rscf.ru/en/project/19-79-30066/). The work was carried out using the equipment of the Joint Research Center of Belgorod State National Research University «Technology and Materials».

№18

IV International Conference and School "Advanced High Entropy Materials" September 26-30, 2022

The effect of aging on microstructure and mechanical properties of VIT-1 alloy

1108668@bsu.edu.ru

Volokitina E.I., Sokolovsky V.S., Salishchev G.A.

Belgorod National Research University, Belgorod, Russia

Introduction

Search for materials that will meet stringent performance requirements is the most important task in the aircraft engine industry. In this regard, alloys based on orthorhombic titanium aluminide (Ti_2AlNb) due to an excellent combination of good workability and oxidation resistance, as well as high specific strength [1]. Meanwhile, one of the main problems hindering the practical application of such alloys is the lack of systematic data on the relationship between their structure and mechanical properties. In particular, the structural and phase transformations during the aging of alloys have not been adequately studied based on orthorhombic titanium aluminide and their effect on mechanical properties [2]. In this regard, the purpose of this work was to study the effect of aging on the evolution of the microstructure and hardness of the VIT-1 alloy.

Materials and methods

The object of study was an alloy with a nominal composition Ti–18,3Al–22,8Nb-1,3Zr-0,3Mo-0,3Ta-0,7W-0,2Si-0,1C (at. %). The material was subjected to forging and the consequent quenching (975 °C, t=2 h, air cooling). Aging was carried out at temperature range (750–850°C) and holding time (0,5;1;2;4;6;8;12;24;48 h).

Results

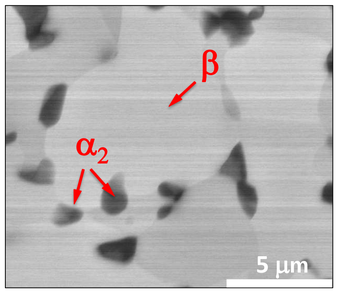

SEM images of alloy after quenching at 975°C for 2 h followed by air cooling

Results

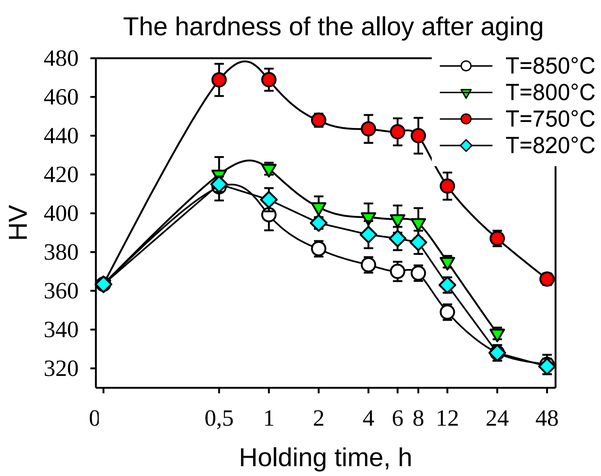

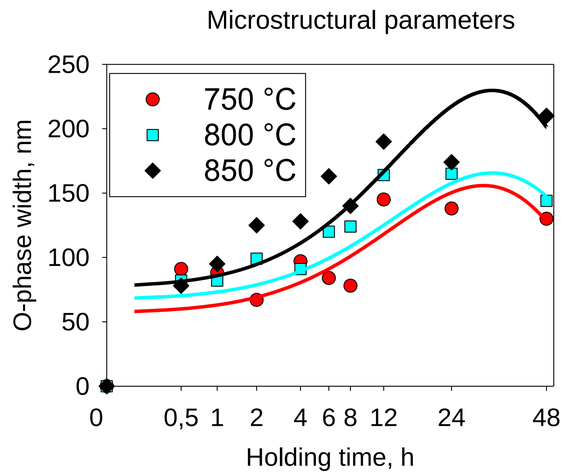

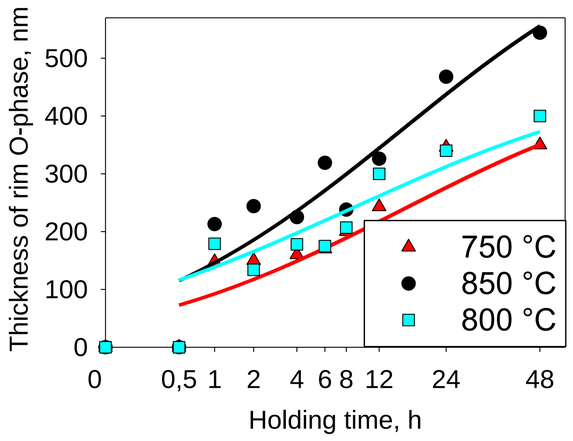

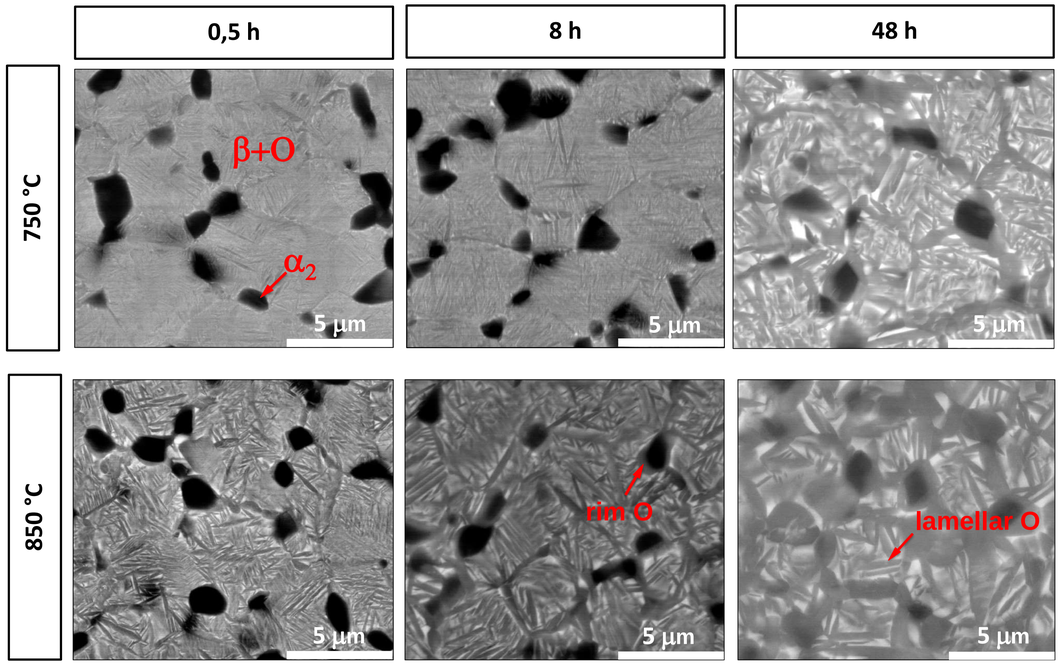

SEM images of the alloy after aging

Conclusion References

The dependence of the hardness of the VIT-1 alloy on the temperature and aging time has been established. It was revealed that aging leads to a sharp hardening of the alloy, followed by softening in two stages. It is shown that: at the first stage, the decrease in the hardness of the alloy under conditions of increasing temperature and aging time occurred due to the coarsening of lamellar particles of the O-phase, at the second stage due to the additional formation and growth of the O-phase and a decrease in the proportion of α_2.

References

1. Kumpfert, J. "Intermetallic alloys based on orthorhombic titanium aluminide." Advanced Engineering Materials 3.11 (2001): 851-864.
2. Chen, W., et al. "Development of Ti2AlNb alloys: opportunities and challenges." Advanced Materials & Processes 172.5 (2014): 23-28.

IV International Conference and School "Advanced High Entropy Materials"
September 26-30, 2022

№19

galkina@bsu.edu.ru

NANOSTRUCTURED COATINGS BASED ON AMORPHOUS CARBON AND CARBON-DOPED WITH GOLD, SILVER AND NITROGEN OBTAINED BY THE PULSED VACUUM-ARC METHOD

Galkina M.E., Kolpakov A.Ya., Poplavsky A.I., Yapryntsev M.N., Novikov V.Yu., Manokhin S.S., Goncharov I.Yu.
Belgorod State National Research University,
85, Pobedy st., 308015, Belgorod, Russian Federation

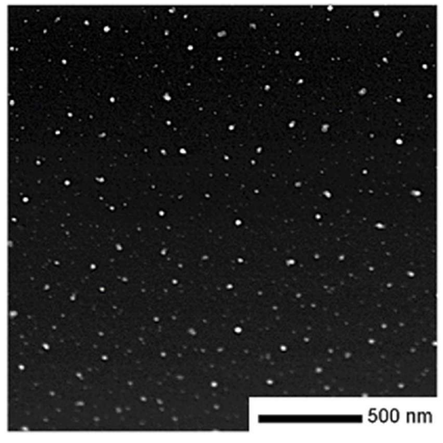

Dark-field PEM image of the carbon coating in the initial state after annealing at 600 °C

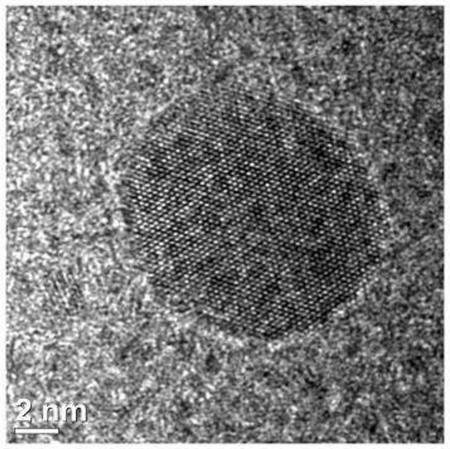

HRTEM images of silver nanocrystallite in the carbon matrix

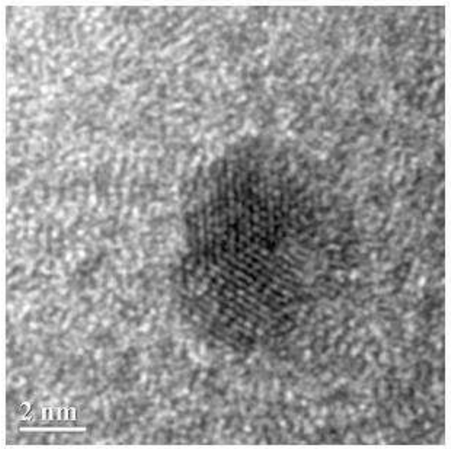

HRTEM image of gold nanocrystallite with the twinning effect

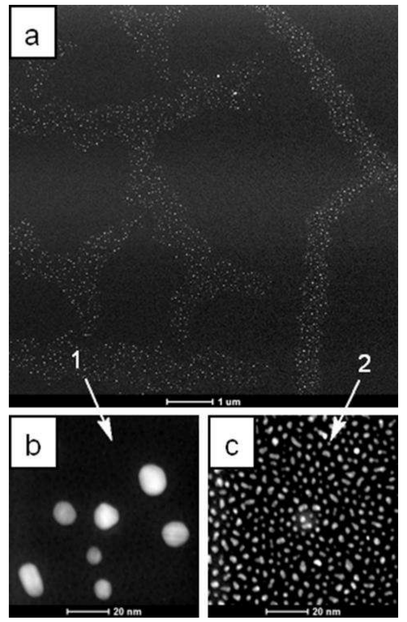

TEM images of a-C:Ag coating revealed local inhomogeneity in the density of distribution of silver nanoclusters. General view of the coating (a), the region 1 of the coating (b), region 2 of the coating (c)

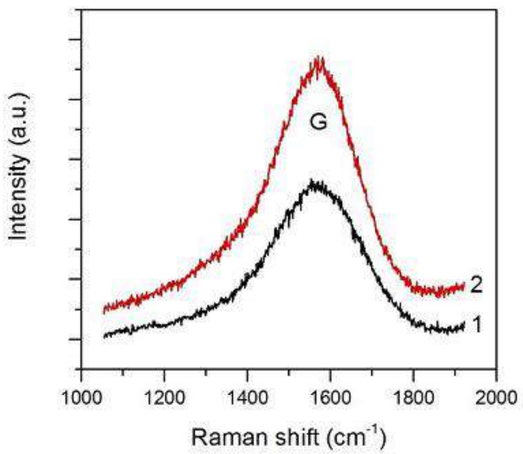

Raman spectra of the carbon coating in the initial state (1) and after annealing in a vacuum at 600 °C (2)

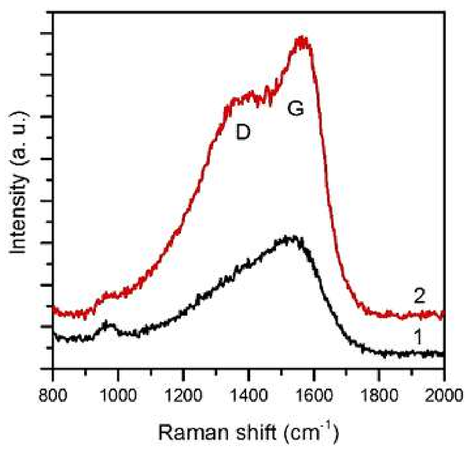

Raman spectra of a-C:Ag coating in the initial state (1) and after annealing at 600 °C (2)

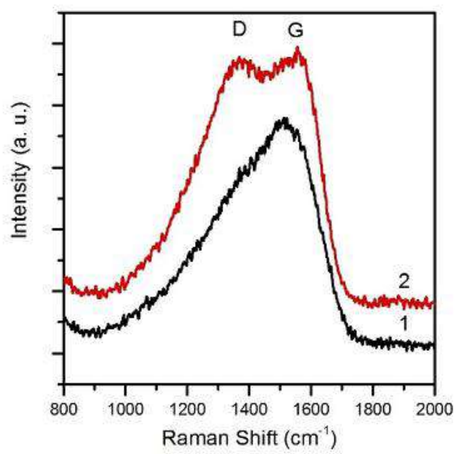

Raman spectra of a-C:N coating in the initial state (1) and after annealing at 600 °C (2)

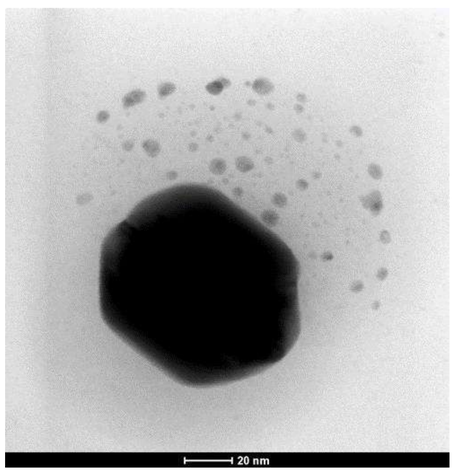

Dark field TEM image of the coalescence of silver nanoclusters in coating a-C:Ag

HIGH VOLTAGE CONSOLIDATION OF POWDER MATERIALS

Grigoryev E. G.

ISMAN, Academician Osipyan str., 8, Moscow Region, Chernogolovka, 142432, Russia eugengrig@ism.ac.ru

Experimental

High-voltage electric discharge consolidation was conducted in a ceramic matrix with diameter 10 mm for cylindrical samples. The applied pressure was 200 MPa, the number of pulses – 1. The value of the applied voltage varied from 5.0 kV to 5.8 kV.

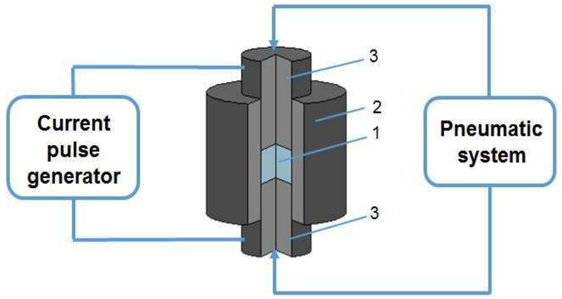

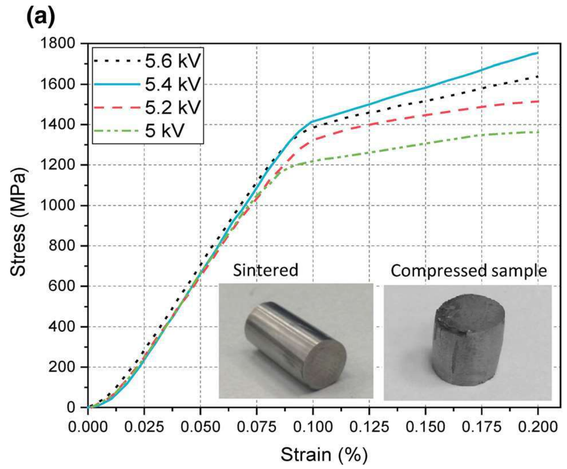

Deformation curves for different modes of the consolidation of a W-Ni-Cu sample

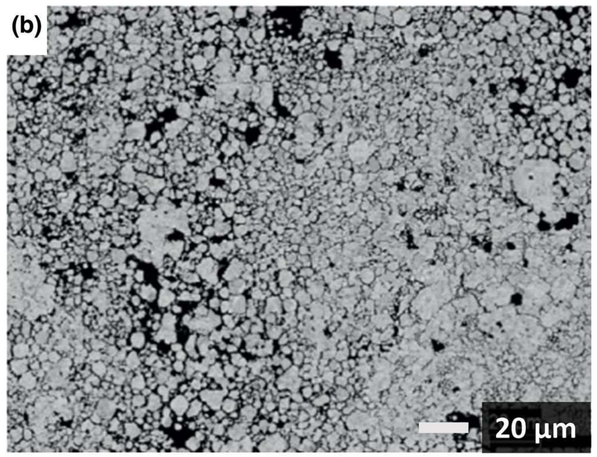

Microstructure of a W-Ni-Cu sample:
blond grains are W and dark regions are Ni, Cu and pores Pressure - 200 MPa, Voltage - 5,2 kV

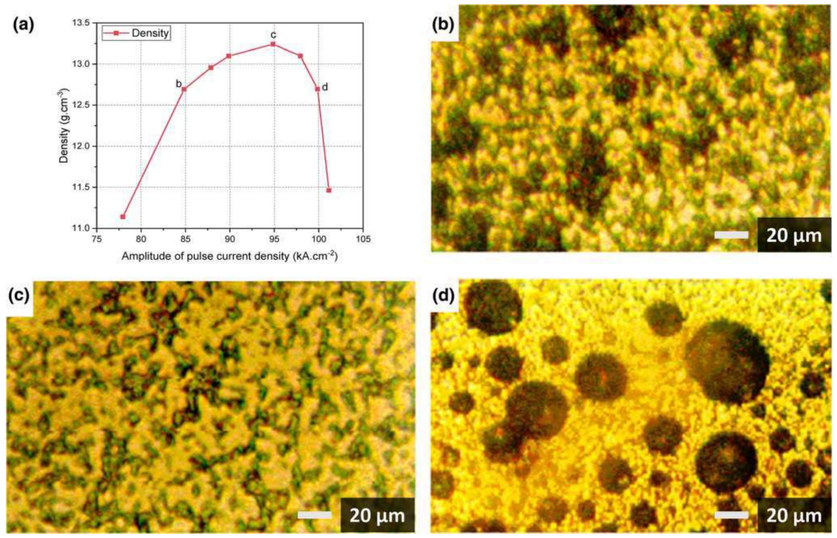

(a) Dependence of the density of the W-20Co samples on the current amplitude, at a pressure of 200 MPa.,
(b), (c), (d) Microstructures of W-20Co samples

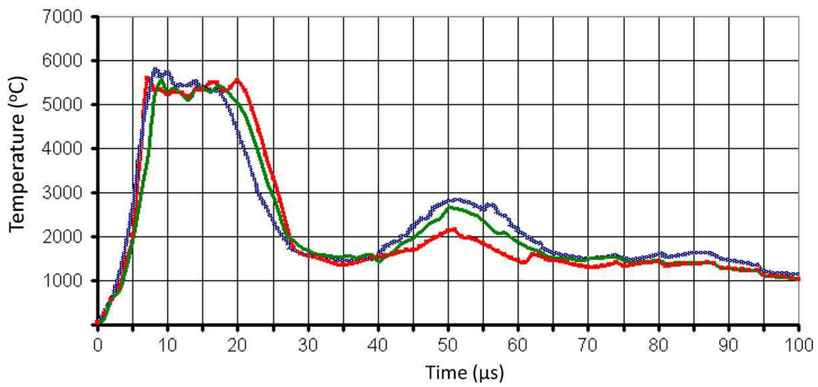

Temperature change of interparticle contacts during HVC.

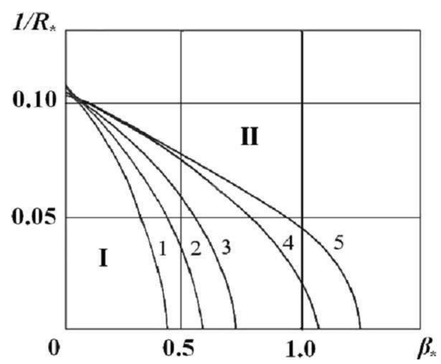

Ranges of values of dimensionless parameters characterizing compaction modes

IV International Conference and School "Advanced High Entropy Materials"
September 26-30, 2022

№ 21

davidovd77@mail.ru

INFLUENCE OF ELEMENTAL POWDER RAW MATERIALS ON THE FORMATION OF THE POROUS SKELETON OF THE MAX PHASE Ti3SiC2 WHEN OBTAINED BY THE NON-VACUUM SHS METHOD

Davydov D.M.
Samara State Technical University

Studies were conducted on the effect on the phase formation, micro- and macrostructure of a porous skeleton based on the MAX-phase Ti3SiC2 obtained by the SHS method in air in backfill from river sand when using various common grades of titanium powders (TPP-7, PTS-1, PTM-1), carbon (C-2, GLS-1, T 900, P 701) and silicon powder (Kr0).

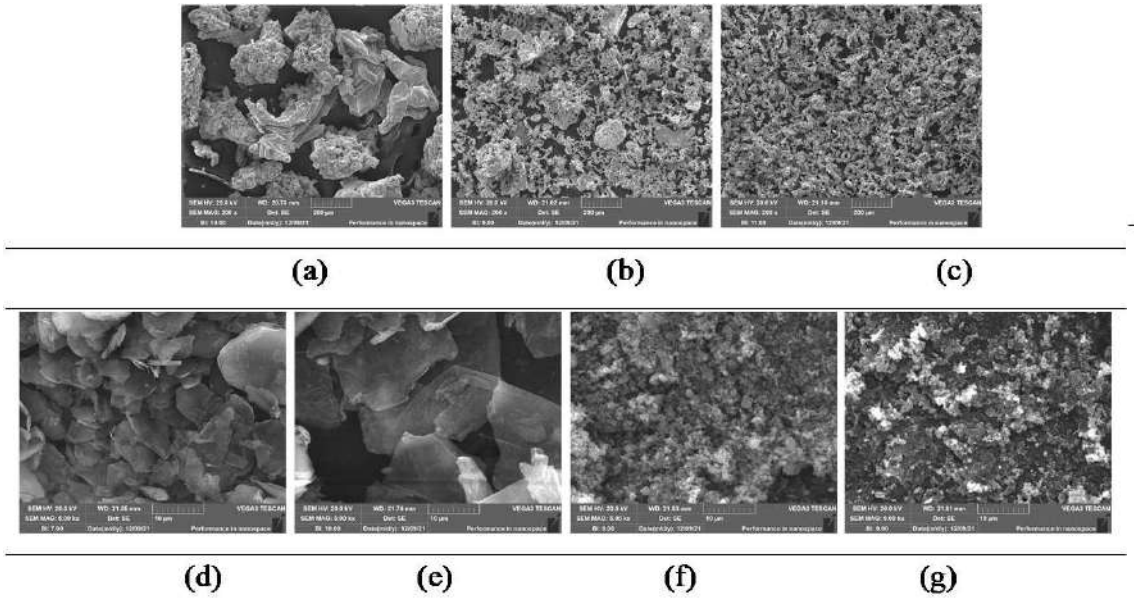

Microstructure titanium powders x 200 (a – TPP7, b – PTS-1, c – PTM-1) and carbon powders x 5000 (d- C-2, e - GLS-1, f - T 900, g - P 701)

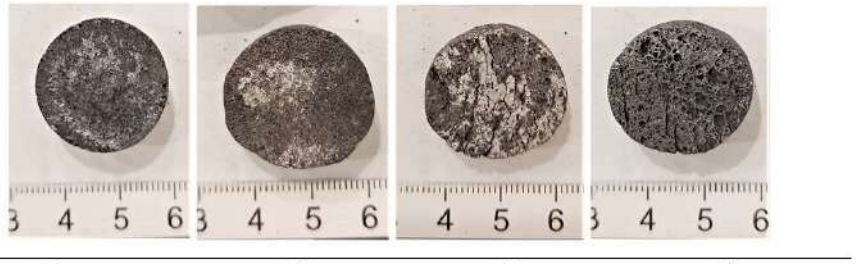

Macrostructure MAX-phase Ti3SiC2 using TPP-7 and carbon (a-C-2, b - GLS-1, c - T 900, d - P 701)

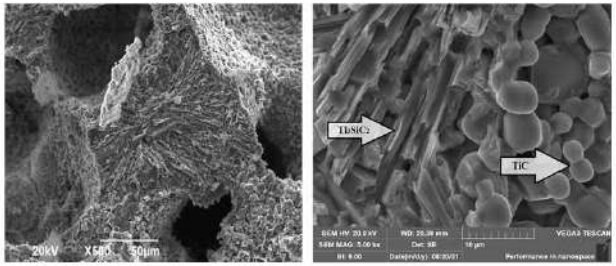

Microstructure MAX-phase Ti2SiC2 (magnification: a – x 500, b – x 5000)

Conclusions:

The density and porosity of the SHS samples obtained from the Ti-Si-C system is most influenced by the shape of the carbon powder. The SHS frame, obtained using a large titanium powder of the TPP-7 brand and graphite powder of the C-2 brand, has the highest of the presented density and compressive strength indicators - 2.41 g/ cm3 and 104 MPa, respectively, and also with a high content of the MAX phase Ti3SiC2 – 66% relative to carbide titan. When using titanium powders of large fraction (TPP-7) and titanium of small fraction (PTM-1) together with graphite powders (C-2) in the initial charge by self-propagating high–temperature synthesis (SHS), the highest indicators in the amount of MAX phase were obtained - 68% and 66%, respectively.

The reported study was funded by RFBR, projects No. 20-08-00435 and No. 20-33-90056.

IV International Conference and School "Advanced High Entropy Materials"
September 26-30, 2022

№ 23

dudova@bsu.edu.ru

CREEP BEHAVIOR OF ADVANCED 9-12%Cr MARTENSITIC STEELS WITH INCREASED BORON AND DECREASED NITROGEN CONTENTS

N.R. Dudova, R.V. Mishnev

9% Cr steels | **Creep behavior** | **10-12% Cr steels**

Boron increase to 80-150 ppm
Nitrogen decrease to 30-100 ppm

→

Enhanced creep resistance in the long-term region at a low stress!
Increased creep rupture strength at 650°C for 100,000 h!

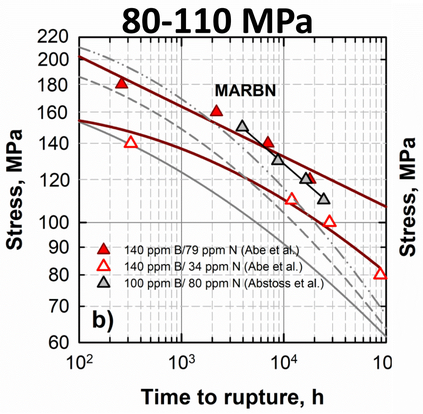

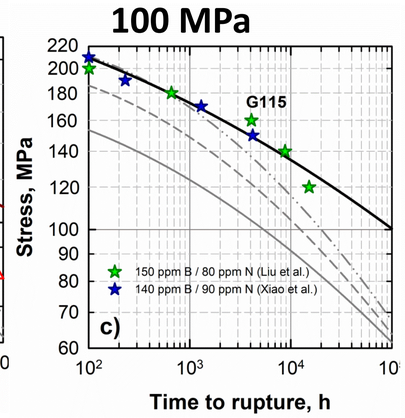

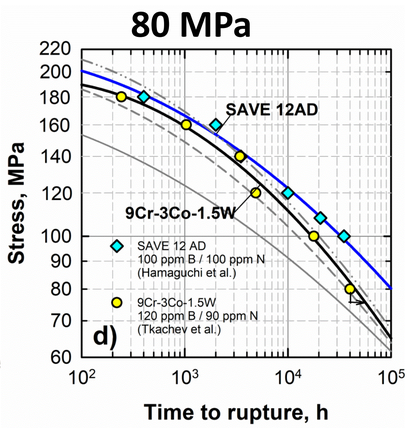

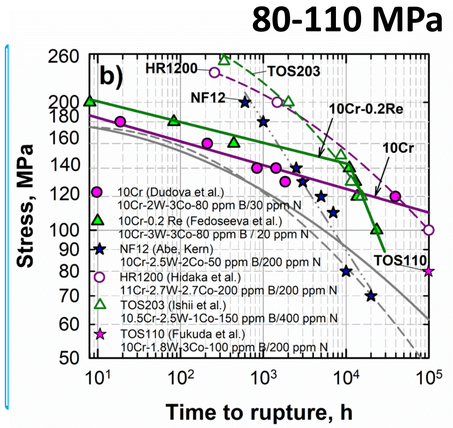

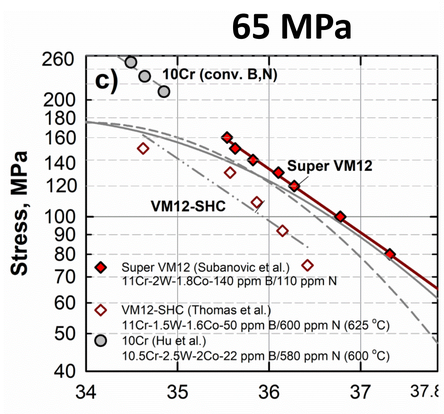

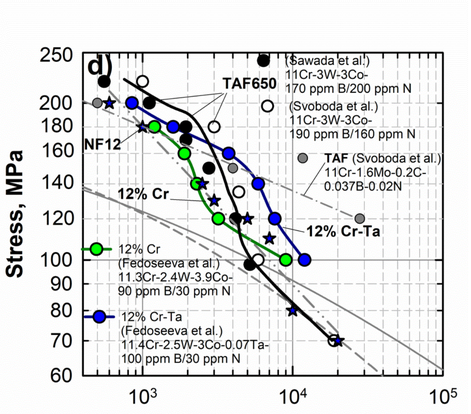

Main factors, improving creep resistance of steels

- No BN formation

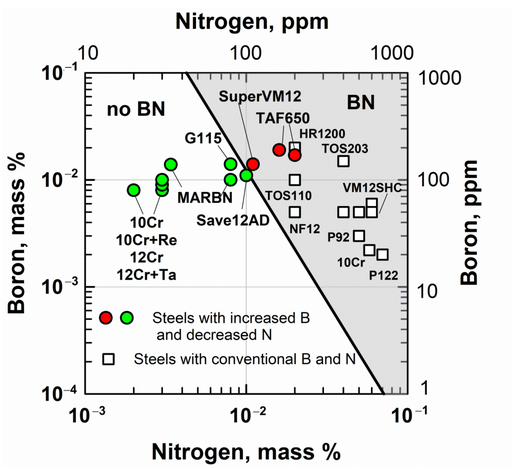

- Enrichment of $M_{23}C_6$ carbides with B

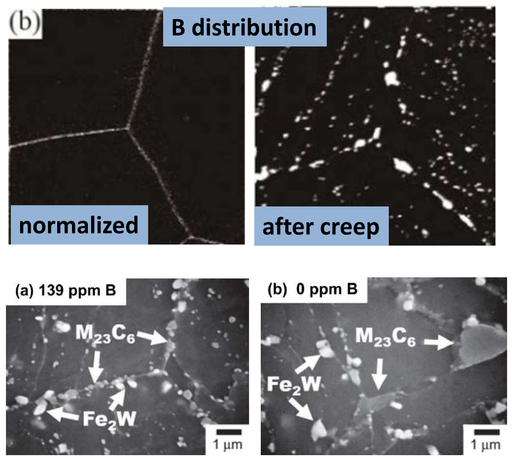

- No intensive coarsening of Laves phase

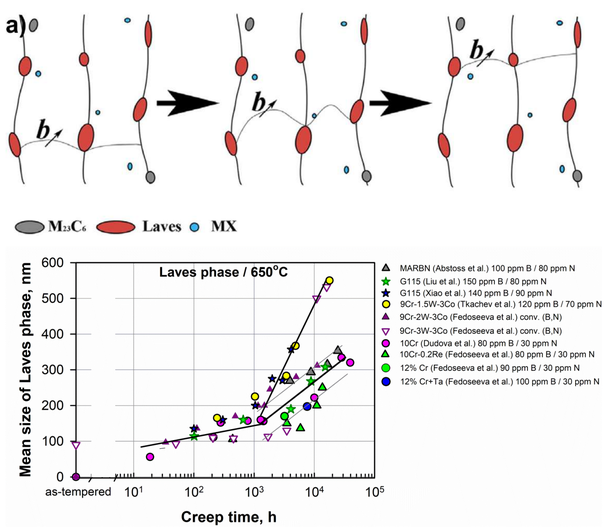

- Additional precipitation of MX

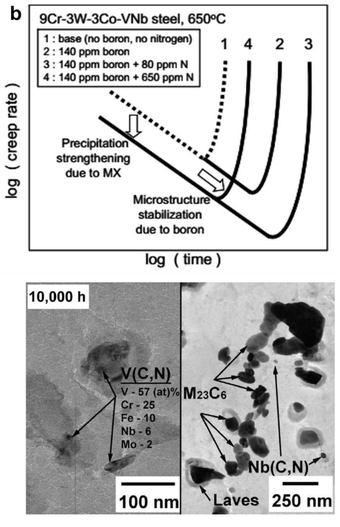

The study was financially supported by the RSF No. 22-29-00145

More detailed information in: Metals 2022, 12(7), 1119; https://doi.org/10.3390/met12071119

IV International Conference and School "Advanced High Entropy Materials"
September 26-30, 2022

№24

SYNTHESIS OF POROUS CERAMIC MATERIALS BASED ON SiC FOR MICROFILTRATION OF LIQUIDS

kira@ism.ac.ru

Kirillov A.O.[1], Uvarov V.I.[1], Kapustin R.D.[1]

[1]Merzhanov Institute of Structural Macrokinetics and Materials Science Russian Academy of Sciences, Chernogolovka, Russia

Subject of research

At present, silicon carbide is a widespread ceramic material with many industrial applications. It has a wide range of unique properties, including high hardness and strength at elevated temperatures, chemical resistance to oxidation, high erosion resistance, etc. The combination of these characteristics makes ceramic porous materials based on silicon carbide one of the most promising in filtration processes for cleaning hot gases, filtration of aggressive liquids and for use as a substrate for catalytic converters in processes of petrochemical synthesis[1].

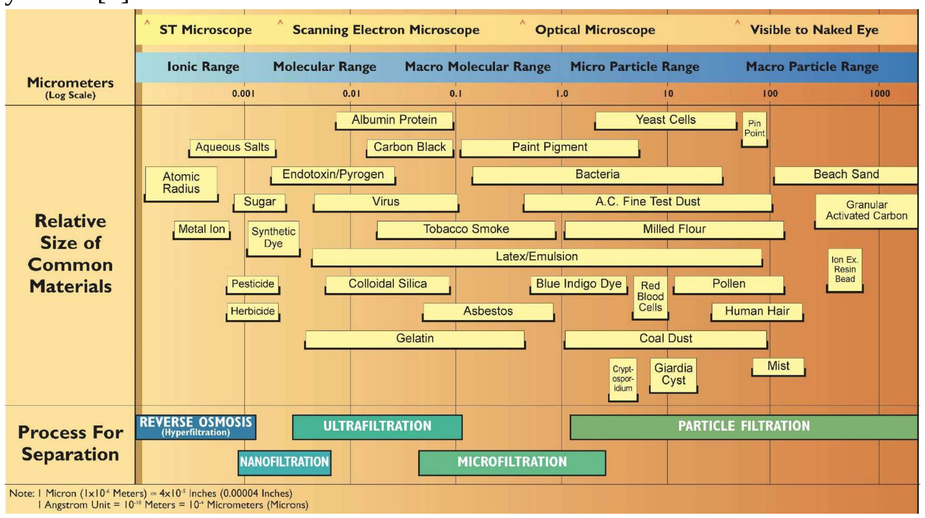

Schematic representation of filtration principles

In general, the technology of ceramic filters production involves the synthesis of materials with their porosity on the order of 30% to 60% and effective permeability. However, depending on the actual operational requirements of the filters, their pore size can significantly vary. The pore size of most porous ceramic materials used in industry ranges from 100 microns to 100 nm. One of the problems is obtaining effective microporous and nanoporous ceramics, since reducing the pore size is usually accompanied by a decrease in the permeability of the material. The search for solutions in this direction is associated with the need to synthesize a porous ceramic material possessing an optimal combination of pore structure and permeability characteristics for microfiltration processes.

Experimental

In this work for obtaining the porous material was used SiC powder with a particle size ~ 7 microns, synthesized by the SHS method, which allowed to obtain a highly developed surface (up to 20 m^2/g). A mixture of powder additives based on magnesium oxides, silicon, etc. was introduced into the charge as a sintering binder. Pressing of the finished mixture was carried out at a pressure of 70 MPa followed by sintering at a maximum temperature of 1300 °C in an air atmosphere.

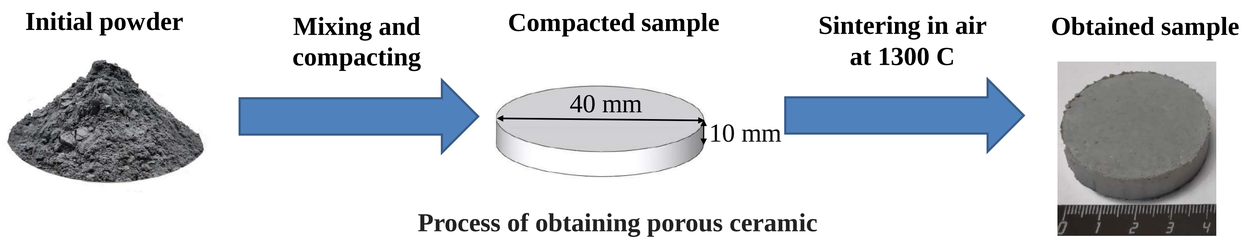

Process of obtaining porous ceramic

The characteristics of the porous material were studied using an Autopore IV 9500 mercury porosimeter by mercury intrusion into the material. The open porosity of the material was 58.5%, mean pore size ~ 384 nm, liquid permeability ~ 0.76 mD, and pore channel tortuosity ~ 59.

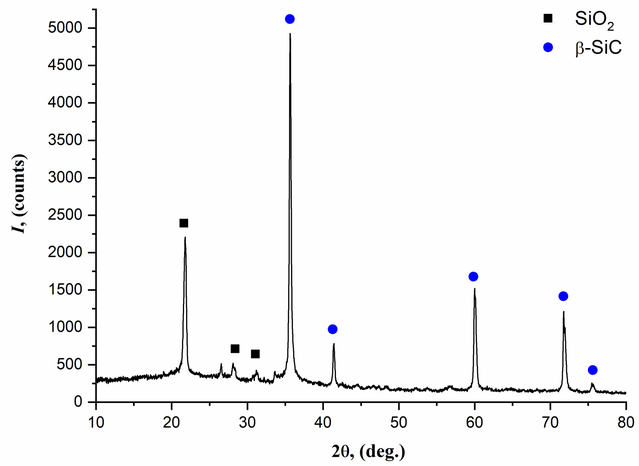

XRD patterns of porous SiC-based ceramic

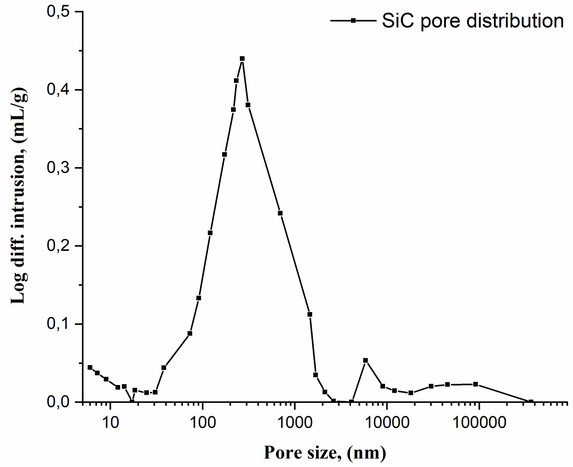

Pore size distribution of sintered ceramic

X-ray analysis showed the presence of a dominant β-SiC phase as well as SiO2, a significant portion of which was formed as a result of SiC oxidation during sintering of the material.

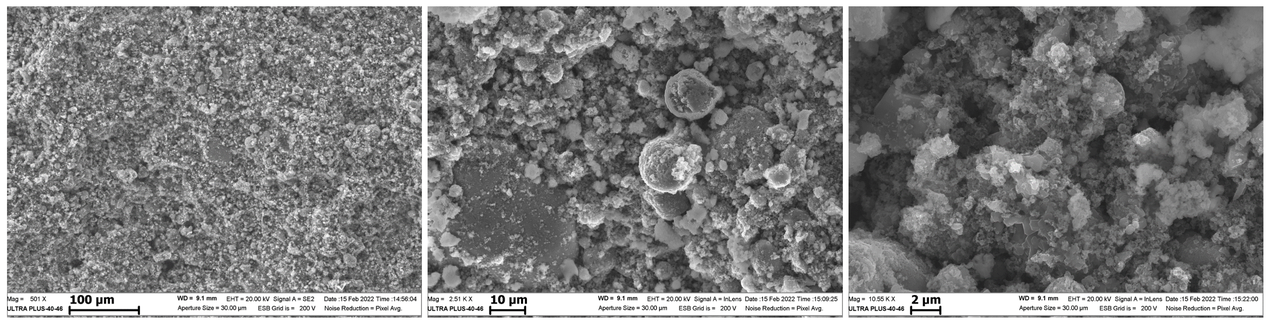

SEM image of fracture surface of porous SiC-based ceramic

The study of the microstructure showed that the synthesized material has a nanoporous structure with a highly developed pore space surface. Thus, the material can be used for production of filters effective in microfiltration processes.

The research was supported financially by the Russian Foundation for Basic Research under the scientific project No. 20-08-00559/22 A.

References

1. Abderrazak H., Hmida E.S.,Silicon Carbide: Synthesis and Properties. Properties and Applications of Silicon Carbide, Janeza Trdine, 2011. 361–388.

IV International Conference and School "Advanced High Entropy Materials"
September 26-30, 2022

№25

kvo@ism.ac.ru

ESTIMATION OF THE IMPACT PRESSURE OF THE FLYER-PLATE WITH A BRONZE BARRIER ACCELERATED BY THE EXPLOSION ENERGY

Kopytskiy V. O., Petrov E. V.
Merzhanov Institute of Structural Macrokinetics and Materials Science Russian Academy of Sciences, Chernogolovka, Russia

Subject of research

The study of the formation of spall cracks in bronze alloys BrAZH9-4 and BrAMc9-2 made it possible to study the processes of plastic deformation under shock wave loading. Shock waves caused by the energy of the explosive creates significant pressure in the material. The impact pressure estimation will make it possible to determine the impulse load level for changing the structure of bronze materials.

To estimate the pressure arising from the collision of an aluminum flyer-plate with the surface of a barrier made of a bronze cylindrical sample (fig. 1), the equation from the work [1] was used. This equation is used in the case of a normal collision during explosion welding of two plates, when at the moment of impact, the plates touches the entire area simultaneously and plane shock waves propagates from the contact surface:

$$p_k = \frac{\rho_2 v_0^2}{\left(\sqrt{1-\rho_2 \mathrm{T}\rho_2^F}+\sqrt{(1-\rho_1 \mathrm{T}\rho_1^F)\rho_2 \mathrm{T}\rho_2^F}\right)} \quad (1)$$

where v_0 – impact velocity; ρ_1 и ρ_2 – initial plate densities; ρ'_1 и ρ'_2 – densities at pressure p_k.

It is possible to calculate the impact pressure of the flyer-plate with the bronze barrier according to the formula (1) only if the velocity v_0 and the equation of metals state are given. The impact velocity was experimentally determined in [2] and it is 1.5 km/s, which correlates with theoretical calculations. Impact adiabats are known for most metals in the pressure range up to 400 GPa. Also, it should be noted that the equations of state of metals have at some point ρ' a bend corresponding to the transition of the medium from an elastic to a plastic state.

The equations of metals state for the flyer-plate and the barrier have the following form:

$$p = A_1\left[\left(\frac{\rho}{\rho_1}\right)^{n_1} - 1\right],\ p = A_2\left[\left(\frac{\rho}{\rho_2}\right)^{n_2} - 1\right] \quad (2)$$

where A_1 и A_2 – constant pressure dimensions; n_1 и n_2 – dimensionless constants.

The values of the impact pressure of the aluminum flyer-plate, accelerated by the explosive ammonite 6ZHV energy, with a bronze barrier, obtained by the equation (1), are about 15-16 GPa. This pressure is several times higher than the shear strength of the studied material.

Experiments

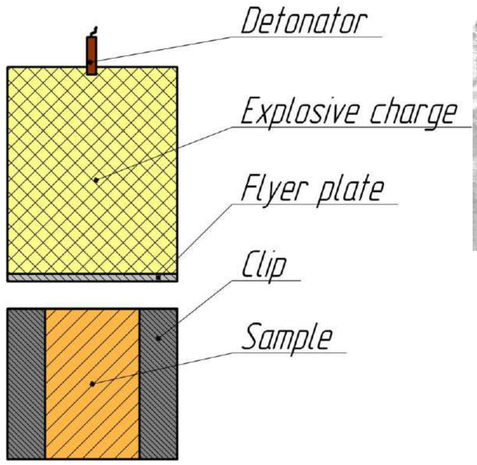

Fig. 1. Experimental scheme of throwing the flyer-plate on the sample

Fig. 2. The appearance of the preserved bronze samples after impact with the flyer-plate

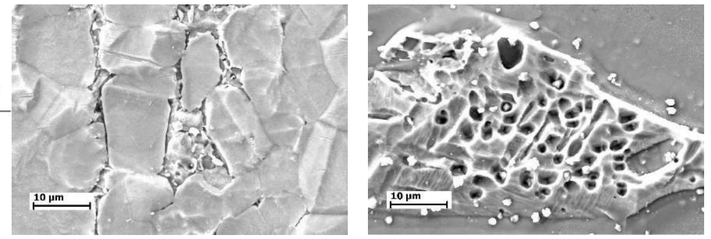

(a) (b)

Fig. 3. Micrographs of the etched surface of bronze microscopic sections after throwing the flyer-plate onto the samples in the clip: a) BrAZH9-4; b) BrAMc9-2

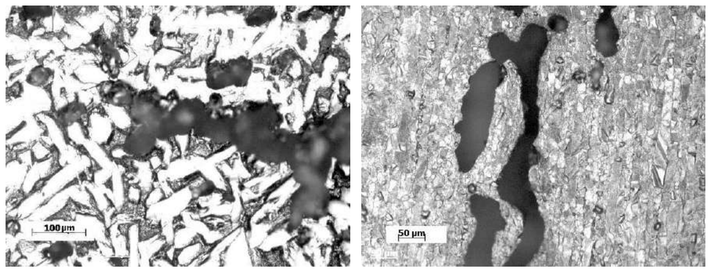

(a) (b)

Fig. 4. Micrographs of the etched surface of bronze microscopic sections after throwing the flyer-plate onto the samples without a clip obtained with an optical microscope: a) BrAZH9-4; b) BrAMc9-2

References

1.Konon Yu.A., Pervukhin L.B., Chudnovskiy A.D. Explosion welding. Moscow, Mashinostroyenie Publ., 1987. 216 p.
2.Kopytskiy V.O. Study of the flyer plate velocity accelerated by the explosion energy // VIII Mezhdunarodnaya konferenciya «Lazernye, plazmennye issledovaniya i tekhnologii» LapLas-2022. Moscow. 2022. p. 226.

IV International Conference and School "Advanced High Entropy Materials"
September 26-30, 2022

№26

numenor@list.ru

seplb1@mail.ru

Macrokinetic analysis of the combustion patterns in the transition from powder to granulated mixtures by the example of 5Ti+3Si and Ti+C compositions

Kochetkov R.A., Abzalov N.I., Seplyarskii B.S., Lisina T.G.

In self-propagating high temperature synthesis processes, even a slight change in the content of impurity gases can lead to a change in the combustion mode and characteristics of the desired products. The influence of both impurity gas release and particle size of the initial components on the combustion velocity of 5Ti + 3Si and Ti + C mixtures is considered. Experimental results are analyzed using a convective-conductive combustion model, which explains the strong effect of impurity gas release on combustion velocity. The usage of the mixtures with a crystalline non-metallic component (Si, C) allowed to reveal the suppressing effect of gases released during heating of titanium particles of different sizes on the velocity of the combustion wave in the mixtures for the first time. The conditions of heating of the initial components in the warm-up zone of the combustion wave in the powder mixture formulated in the work allowed predicting whether the combustion rate of 5Ti + 3Si and Ti + C mixtures during the transition from powder to granular mixtures will increase or decrease. Unlike powder mixtures, a monotonous decrease in the rate of combustion of granular mixes with an increase in the total particle size of the initial components is associated with leveling the effect of impurity gas release. The values of combustion velocities of granular mixes are approximated by the same power dependence on the total particle size of the initial components for both compositions; it corresponds to the linear law of interaction of the initial components in the theory of flame front propagation in a condensed heterogeneous medium.

Table.1 Characteristics of the initial components

The initial substances used in this work and their brief characteristics are given in Table 1. For convenience of presentation, the designations (m) are used below for smaller and (k) for larger particle sizes of the initial powders. We also used narrow fractions screened out from the initial fraction of titanium Ti(c), with particle sizes <40 μm, 40–80, 90–125, and 125–200 μm, designated Ti (c)-I, Ti(c)-II, Ti(c)-III, Ti(c)-IV, respectively.

Component	Trade mark	Particle sizes, μm	
		up to 50 wt%	up to 90 wt%
Ti	PTM-1 (m)	< 34	< 54
	PTM-1 (k)	< 105	< 169
Si	P/p (m)	< 2.1	< 6.5
	P/p (k)	< 8	< 22
Carbon (graphite)	Aldrich	< 5	< 14
Polyvinylbutyral			
Technical ethyl alcohol 95%			

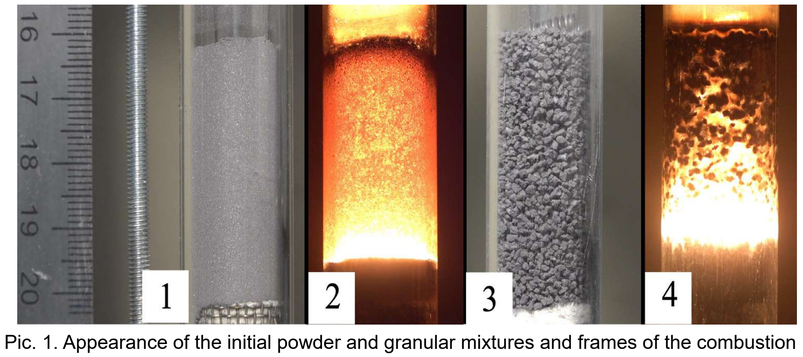

Pic. 1. Appearance of the initial powder and granular mixtures and frames of the combustion process

Table 2. Average velocities of the combustion front of investigated mixtures.

Mixture No	Initial components		Combustion velocity, mm/s	
			powder	granules
1	Si (k)	Ti (k)	20	16
2		Ti (m)	15,5	24
3	Si (m)	Ti (k)	25	17.5
4		Ti (m)	21	29
5		Ti (k) -I	30	39
6		Ti (k) -II	38	25
7		Ti (k) - III	21	18
8		Ti (k) - IV	20	13.5
9	C	Ti (m)	20	25
10		Ti (k) -I	25	30
11		Ti (k) -II	10	20
12		Ti (k) - III	7.5	15
13		Ti (k) - IV	6	11

We assume that the particles of initial components have time to get warmed thoroughly before the combustion front if the two following conditions are met. (Note that the experimental results given below confirm that such heating conditions are correct.) First, the characteristic particle size d should be less than the warm-up zone width $L = a_c / u$, where u is the experimental combustion velocity and a_c is the temperature conductivity of the heterogeneous powder mixture (1).

Second, the thermal relaxation time of the particle $t_h = d^2/4a$ (a is the thermal conductivity of the particle) should be less than the characteristic time of its location in the warm-up zone $t = L/u = a_c/u^2$ (2)

$$d < L \qquad (1)$$

$$t_h < t \qquad (2)$$

The results of the verification of conditions (1), (2) for initial components of the powder mixtures are shown in Table 3. The sign (+) means that the warm-up conditions are satisfied, (-) indicates the opposite situation. In the calculations of L and t, the experimental combustion velocities shown in Table 2 were used.

As is seen in Table 3, for non-metallic components Si and C, the warm-up conditions are met, therefore impurity gas (IGR) release from these (if any) occurs before the combustion front for all powder mixtures and reduces the propagation velocity of the combustion front. Thus, the combustion patterns of the investigated mixtures being discussed are determined by the features of heating of titanium particles.

For granular SHS compositions, it should be noted that granulation contributes to the leveling of the effect of IGR !

Table 3. The fulfilment of warm-up conditions (1), (2) of initial components in combustion of powder mixtures .

Mixture No	Initial components		Powder mixture	
	Ti	Si, C	L, μm	t, $c \cdot 10^3$
1	-	+	50	2.5
2	+	+	65	4.2
3	-	+	40	1.6
4	+	+	48	2.3
5	+	+	33	1.1
6	-	+	26	0.7
7	-	+	48	2.3
8	-	+	50	2.5
9	+	+	50	2.5
10	+	+	40	1.6
11	+	+	100	10
12	+	+	133	18
13	+	+	167	28

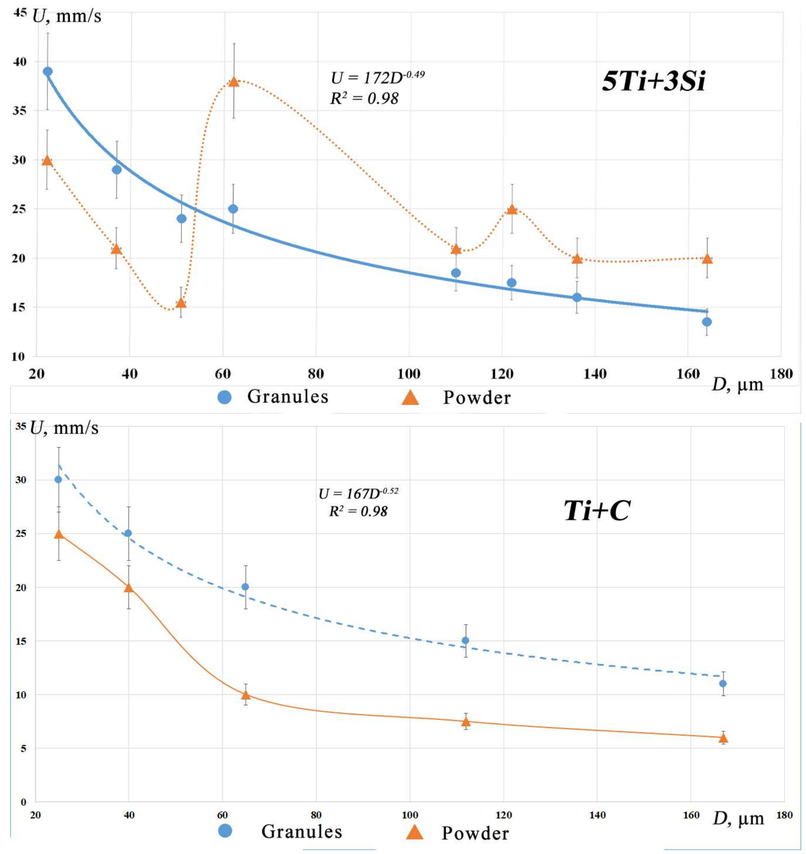

Pic. 2. The dependence of combustion velocities of powder and granular mixtures of 5Ti + 3Si and Ti+C on the total size of the initial components.

Conclusions

The changes in the combustion rate during the transition from powder to granular mixtures of 5Ti + 3Si and Ti + C (graphite) were experimentally determined for the first time by varying the dimensions of the initial reagents.

The obtained results are explained from the point of view of a convective-conductive model of combustion, which takes into account the effect of impurity gas release on the combustion velocity.

The conditions for heating particles of powder mixtures in the warm-up zone of the combustion wave have been formulated and experimentally confirmed for the first time.

Approximation dependence of combustion rate u of granulated mixtures on the total particle size of initial components D is obtained, which turned out to be qualitatively the same for 5Ti + 3Si and Ti + C mixtures and has a form $u \sim D^{-1/2}$.

IV International Conference and School "Advanced High Entropy Materials"
September 26-30, 2022

№27

E-mail:
petr@ism.ac.ru

MATHEMATICAL MODELING COMBUSTION OF LAYERED CONDENSED MEDIA TAKING INTO ACCOUNT THE DIFFUSION MIXING OF THE REACTANTS

Krishenik P.M.*, *Rogachev S.A.*, *Shkadinskii K. G.* **Institute of Structural Macrokinetics and Materials Science, Russian Academy of Sciences, Chernogolovka**
***Institute of Problems of Chemical Physics, Russian Academy of Sciences, Chernogolovka**

More information can be found in the article: Int. J. Self-Propag. High-Temp. Synth., 2021, Vol. 30, No. 1, pp. 5–10. DOI: 10.3103/S1061386221010131

Introduction

Earlier studies on combustion wave propagation along the interface in bilayer systems [1, 2] have shown that critical conditions for combustion of such systems are defined by bilayer thickness and heat sink into environment.

In this communication, we report on mathematical modeling of combustion wave propagation in between two reactive layers with due regard for melting and interdiffusion of reagents and special emphasis on critical conditions for steady wave propagation, interdiffusion of melted reagents, and onset of oscillation combustion modes.

It is assumed that one-stage combustion reaction compounds C_1 and C_2 yields product C.

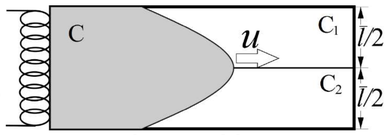

Fig. 1. Schematic of the system under consideration

Chemical reaction gets started only after the interdiffusion of melted reagents, i.e. reaction rate is defined by reagent concentrations C_1, C_2 and running temperature T. After ignition with a coil warmed up to temperature T_m, a combustion wave propagates along the interface between compounds C_1 and C_2 at burning velocity u. Each layer undergoes melting at one and the same melting point T_m. The melt is characterized by the function η defined as the volume fraction of liquid phase per a volume unit. For $T < T_m$, the interdiffusion is negligibly low; whereas for $T > T_m$, diffusivity D spasmodically grows. The problem will be formulated without explicit definition of interface as suggested in [3, 4]. Phase transformation is replaced by non-isothermic "chemical" reaction when the process of phase formation takes place within a "narrow" layer.

[1] A. S. Rogachev, A. S. Vadchenko, and A. S. Mukasyan, Advances in Science and Technology. 88: 85-93. 2014.
[2] A. S. Rogachev, Russ. Chem. Rev., 77(21): 21-37. 2008.
[3] I. S. Gordopolova, T. P. Ivleva, K. G. Shkadinsky, and V. I. Yukhvid, Int. J. Self-Propag. High-Temp.Synth., 10(20). 2001. 177–181.
[4] A. P. Aldushin, A. G. Merzhanov, Dokl. Akad. Nauk SSSR,. 236(5), 1977. 1133–1136, doi: 10.1006/jcph.1995.1039.

Mathematical model

Equation of heat conduction:

$$\frac{\partial\theta}{\partial\tau} = \frac{\partial}{\partial\xi}\left(\frac{\partial\theta}{\partial\xi}\right) + \frac{\partial}{\partial\psi}\left(\frac{\partial\theta}{\partial\psi}\right) + c_1c_2\exp[\theta/(1+\beta\theta)] - \Delta_k\Delta_Q F(\eta,\theta)$$

Equation of diffusion (with account for consumption of C_1 and C_2):

$$\frac{\partial c_1}{\partial\tau} = \frac{\partial}{\partial\xi}\left(\mathrm{Le}\frac{\partial c_1}{\partial\xi}\right) + \frac{\partial}{\partial\psi}\left(\mathrm{Le}\frac{\partial c_1}{\partial\psi}\right) - \gamma c_1c_2\exp[\theta/(1+\beta\theta)]$$

$$\frac{\partial c_2}{\partial\tau} = \frac{\partial}{\partial\xi}\left(\mathrm{Le}\frac{\partial c_2}{\partial\xi}\right) + \frac{\partial}{\partial\psi}\left(\mathrm{Le}\frac{\partial c_2}{\partial\psi}\right) - \gamma c_1c_2\exp[\theta/(1+\beta\theta)]$$

where $\mathrm{Le} = \begin{cases} \mathrm{Le}_0 \text{ for } \theta \ge \theta_m \\ 0 \quad \text{for } \theta < \theta_m \end{cases}$

Boundary conditions:

$$\theta(\psi,0,t) = \theta_{in} \quad \tau \le \tau_{imp} \qquad \frac{\partial\theta(\psi,0,\tau)}{\partial\xi} = 0 \quad \tau > \tau_{imp}$$

$$\frac{\partial\theta(\xi,0,\tau)}{\partial\psi} = \alpha(\theta-\theta_0) \qquad \frac{\partial\theta(\xi,l,\tau)}{\partial\psi} = \alpha(\theta-\theta_0)$$

Initial conditions:

$$\theta(\xi,\psi,0) = \theta_0 \quad \eta(\xi,\psi,0) = 0$$

$$\begin{cases} 0 \le y \le l/2: & c_1(\xi,\psi,0) = 1, c_2(\xi,\psi,0) = 0 \\ l/2 < y \le l: & c_1(\xi,\psi,0) = 0, c_2(\xi,\psi,0) = 1 \end{cases}$$

Phase transformations (melting ↔ solidification) within the layer described by the following equation

$$F(\eta,\theta) = \frac{\partial\eta}{\partial\tau} = \begin{cases} k_m(1-\eta)\mathrm{sign}(\theta-\theta_m)\exp(|\theta-\theta_m|\Delta) & \text{for } 0<\eta<1 \\ 0 \quad \text{for } \eta = 0 \quad \text{or} \quad \eta \ge 1 \end{cases}$$

θ temperature, θ_{in} temperature of reaction initiation, τ time, ξ and ψ spatial coordinates, $\beta = (RT_*)/E$; $\gamma = (RT_*^2c)/EQ$; $\mathrm{Le}_0 = c\rho D_0/\lambda$.

Mathematical model was analyzed numerically by the method of varied directions using a 2D rectangular grid. Implicit three-point approximation of second derivatives afforded for regulating time pace on retention of accuracy and scheme stability. Time pace depended on heat release rate and temperature.

Results and discussion

Figure 2 shows the distribution of temperature θ and product concentration c over the (ξ,ψ) plane in case of steady combustion. A stable combustion front with a 'narrow' reaction zone and uniform temperature distribution across the bilayer is formed in case of 'thin' layers ($l \le 10$). With increasing l, the combustion front becomes curved (see Fig. 2a). The surface of chemical transformation is characterized by the isoline c = 0.5(Fig. 2 b). Behind the narrow reaction zone, we observe the interdiffusion of reagents and their reaction.

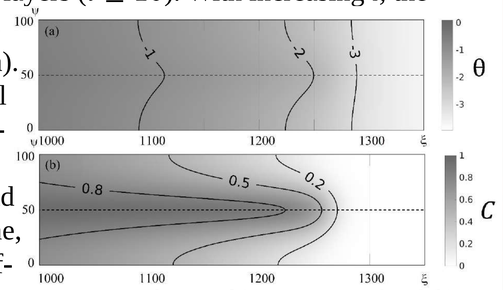

Fig2. Distribution of (a) temperature θ and (b) product concentration c

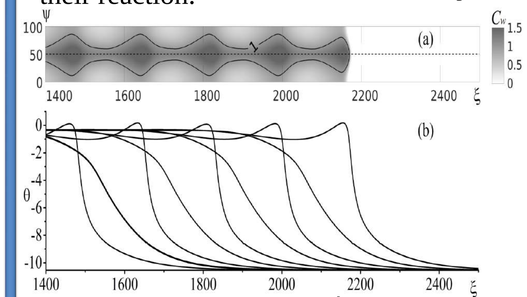

Fig. 3. (a) Function $c_w = -\int_0^{\tau_{max}} \frac{\partial c_1c_2}{\partial\tau}(\theta-\theta_0)d\tau$ and (b) temperature θ as a function of ξ

Figure 3a shows the c_w function for a sample burned in an oscillation mode. At the moment of 'burst' (Fig. 3b), temperature grows, and this leads to the acceleration of the reaction and hence to higher extent of conversion. Accordingly, the oscillation combustion mode yields a product with periodic inhomogeneities in its structure. Figure 4 presents volume fraction η of liquid phase and temperature θ as a function of ξ in conditions of strong heat losses ($\alpha \to \infty$). In the presence of heat loss, the bilayer is not melted throughout (Fig. 4a). The melted domain moves ahead along with the combustion front (Fig. 4b). Lateral heat losses lead to the formation of unreacted layer.

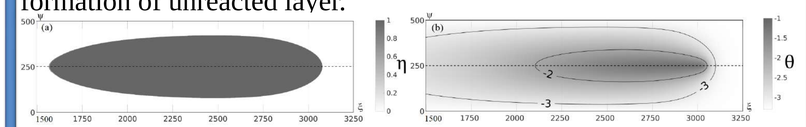

Fig. 4. (a) Volume fraction of liquid phase η and (b) temperature in conditions of heat losses.

IV International Conference and School "Advanced High Entropy Materials"
September 26-30, 2022

№ 31

lisinatg@gmail.com

B.S. Seplyarskii, R.A. Kochetkov, T.G. Lisina, and N.I. Abzalov

Comparative Investigation of Macrokinetic Parameters Of Diluted (Ti+C)-based Powder and Granular Mixtures

Component		Particle size, μm	
		< 50% wt.	< 90% wt.
Titanium	Ti	< 105	< 169
Nickel	Ni	<14.3	<27.5
Cuprum	Cu	<38	<72
Carbon (soot)	C	< 1	< 2
Polyvinyl butyral			
Industrial alcohol 95%			

Starting materials ↑ for powder and granular samples (1% of polyvinyl butyral as a binder) and mixtures ↓

№	Mixture	%Ti	%C	T_{ad}, K	T_c, K
1	Ti+C	80	20	3300	2950
2	(Ti+C)+20%Ni	64	16	3050	2400
3	(Ti+C)+20%Cu	64	16	3850	2550
4	(Ti+C)+20%TiC	64	16	3000	2350
5	(Ti+C)+20%Ti	84	16	2950	2750

Thermodynamic calculation (THERMO software http://www.ism.ac.ru/thermo) gives titanium carbide and metal as the only combustion products of mixtures 2, 3. Therefore, Ni and Cu additives to the Ti+C mixture can be considered as inert diluents as TiC. Experiment: $T_c(1)>T_c(3)>T_c(2)$ when $U_a(1)<U_a(2)$, $U_a(1)<U_a(3)$ → In accordance with Convective-Conductive Model of Combustion*, the front movement is retarded with impurity gases released from powder particles before the front. Conditions of desorption and particles warming ahead of the front are: (1) mean particle size of reagent d is smaller than the width of the warm-up zone $L = a/U_a$ (where a is thermal diffusivity of powder blend), (2) thermal relaxation time $t_h = d^2/4a_1$ for a powder particle (a_1 is thermal diffusivity of particle material) is smaller than its dwell time $t = L/U_a = a/U_a^2$ within the warmup zone. The heating conditions (1), (2) are met in Blends 1, 4, 5 and are not met in Blends 2 and 3 → That explains measured velocities of combustion front in powder mixtures 2 and 3. As heated depth of a granule till its ignition (0.15-0.22 mm for D=0.6 mm and 0.25-0.31 mm for D=1.7 mm) is much smaller then granule size D, the combustion velocity inside individual granule U_d and the combustion transfer time between the granules t_{ig} can be considered equal for granules of different size (provided the granules retain their size upon synthesis ↓). Two expressions for $U(D)$ in a granular mixture $U(D) = U_d/(1 + U_d t_{ig}/D)$ written for two various D form a system of equations for obtaining U_d and t_{ig}. U_d exceeds U_a for all blends ↑. Maximum retarding effect U_d/U_a is not in a mix 5 (84% Ti), but in mix 4. This indicates a significant release of impurity gases from titanium carbide particles.

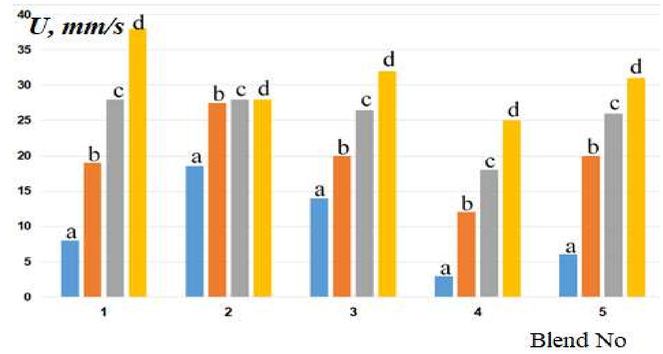

↑ Velocity in Powder (a), Granular 0.6 mm (b)/1.7 mm (c) mixes, velocity inside granules (d)
↓ Fulfillment (+/-) of warmup conditions for metal and carbide particles

№	U_a, mm/s	Component	d, μm	L, μm	t_h, 10^3 s	t, 10^3 s	+/-
1	8	Ti	120	125	0.450	16	+
2	18.5			54	0.450	3	-
3	14			71	0.450	5	-
4	3			333	0.450	111	+
5	6			167	0.450	28	+
2	18.5	Ni	15	54	0.004	3	+
3	14	Cu	40	71	0.027	5	+
4	3	TiC	23	333	0.021	111	+

Example of (Ti+C)+20%Cu sample (the shots for other mixtures look quite similar) ↓

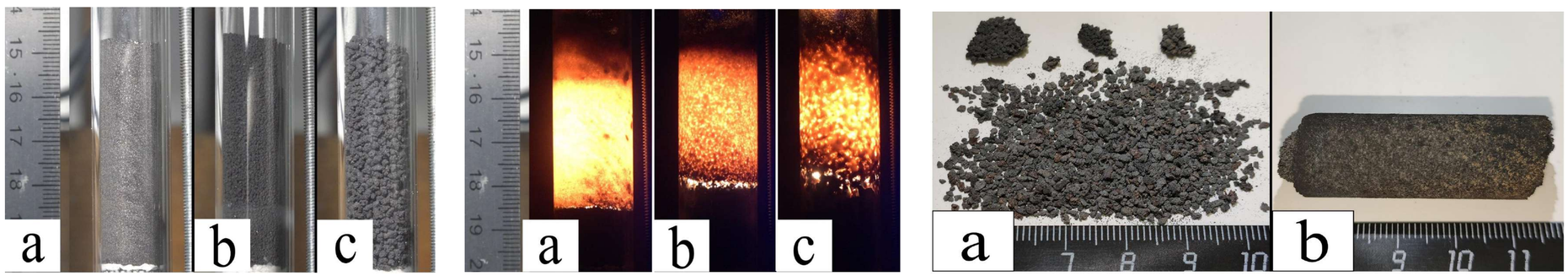

Powder (a) and Granular 0.6 mm(b)/1.7 mm(c) samples and shots of combustion. Products of synthesis of granular and powder mix.

*Rubtsov, N.M., Seplyarskii, B.S., and Alymov, M.I., The convective–conductive theory of combustion of condensed substances, in Ignition and Wave Processes in Combustion of Solids, Springer, 2017, pp. 117–171. https://doi.org/10.1007/978-3-319-56508-8_4

Resume Combustion velocity inside the granules, time of combustion transition between the granules, and quantitative assessment of the retarding effect of impurity gases in powder mixtures were obtained for 5 mixtures. Unusual velocities values in diluted mixtures were explained. Impurity gases reabsorption by titanium carbide was confirmed.

IV International Conference and School "Advanced High Entropy Materials"
September 26-30, 2022

№33

E-mail:
artyom.litvinko@gmail.com

PRODUCTION OF BRIQUETTES AND METALLURGICAL COMPOSITES FROM METAL-WORKING WASTE

A.A. Litvinko
Belarusian National Technical University, Minsk, Republic of Belarus

The technology proposed for implementation in this work includes the following technological operations:

- separation of waste in order to remove foreign objects, crushing, batch preparation by mixing components;
- non-oxidizing heating of the charge to temperatures of incomplete hot deformation (700-800 ℃) in an atmosphere of products of thermal sublimation and pyrolysis of the oil component of the cutting fluid (coolant);
- formation of a pyrocarbon coating on the surface of metal particles, which protects the metal from oxidation and acts as a lubricant in the hot pressing process;
- combustion of oil vapors together with natural gas, flue gas cleaning in a Venturi scrubber, catalytic afterburning of CO, condensate collection and hydrocarbon regeneration;
- supply of hot charge into the mold with minimal heat loss (no more than 15-20 ℃);
- pressing on a hydraulic press under a pressure of 470-500 MPa in a mold with a movable matrix that activates the action of lateral friction forces directed towards the current pressing force;
- production of briquettes and metallurgical composites with a density of at least 90% of the density of castings of the same chemical composition.

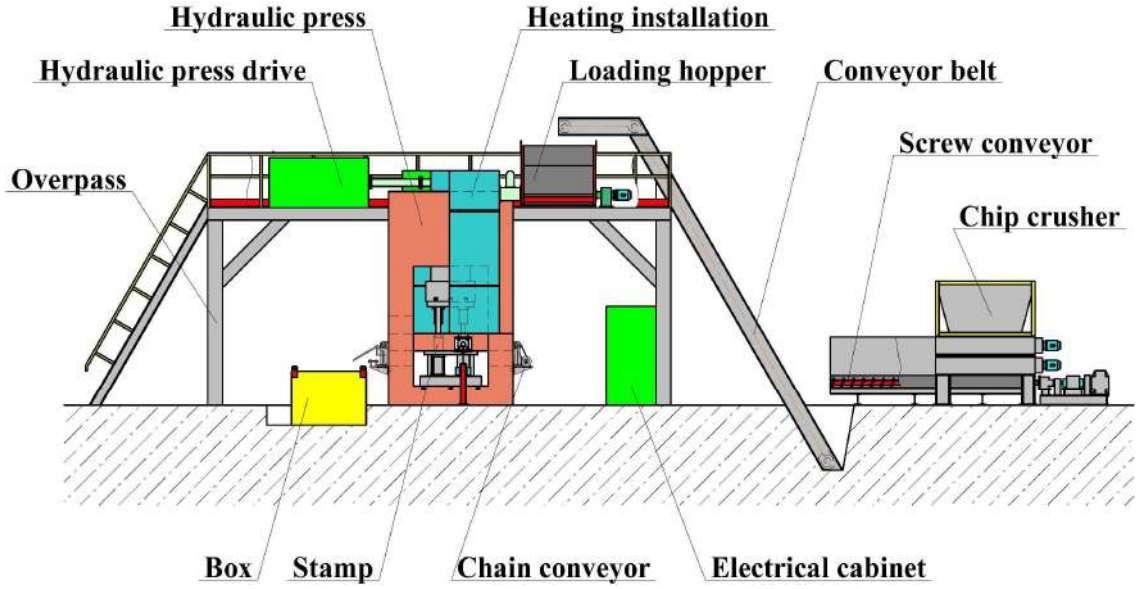

Figure 1. Technological line of hot briquetting

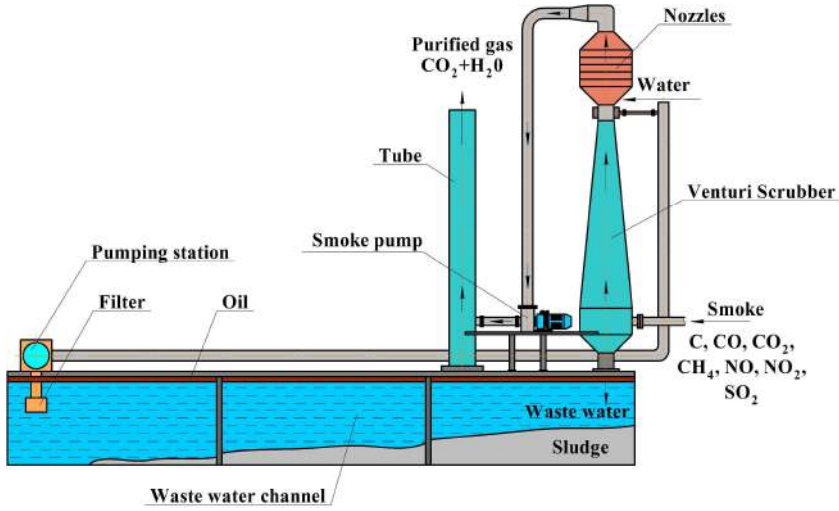

Figure 2. Gas purification scheme

The technical and economic result of the proposed technology:

- the complete removal of residual moisture and organic impurities from metal waste;
- the elimination of decarburization and waste metal, its fine fractions (up to 1 mm);
- the use of sludge powders, slag-forming and alloying additives in the composition of briquettes;
- the production of high-quality briquettes - substitutes for overall lump scrap and cast billets;
- reduction of energy and transport costs for the production of briquettes and their processing.

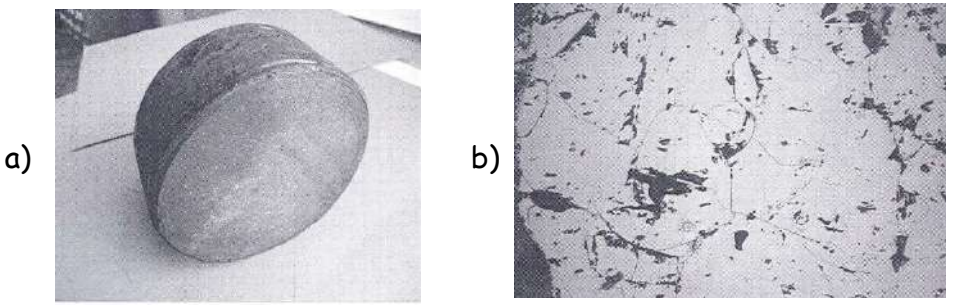

Figure 3. a) Appearance of a hot-pressed briquette;
b) microstructure of the briquette

IV International Conference and School "Advanced High Entropy Materials"
September 26-30, 2022

№34

E-mail Olga.Malyshkina@mail.ru

Malyshkina O. V., Mamaev D.V., Ivanova A.I.

Тверской государственный университет

The effect of the tellurium vapor on the structure formation and dielectric properties of a multi-component system based on sodium-potassium niobate

A multicomponent system based on sodium–potassium niobate ceramics (mKNN) with the general formula $(Na_{0.5}K_{0.49}Li_{0.05}Sr_{0.05})(Nb_{0.9}Ta_{0.05}Ti_{0.05})O_3$ was obtained by solid-phase synthesis.

mKNN

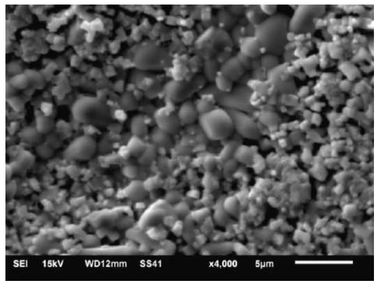

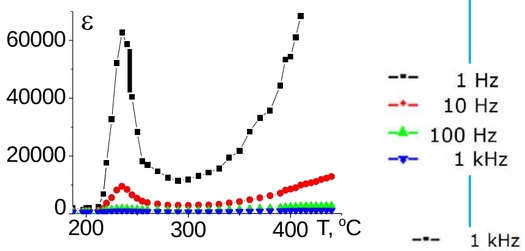

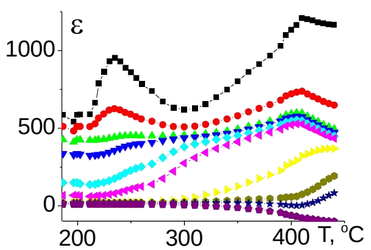

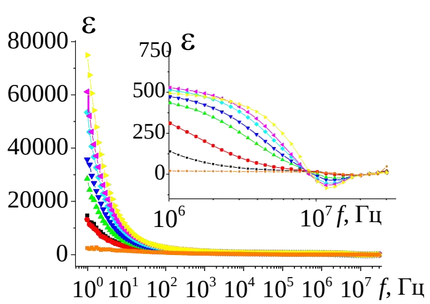

5 μm

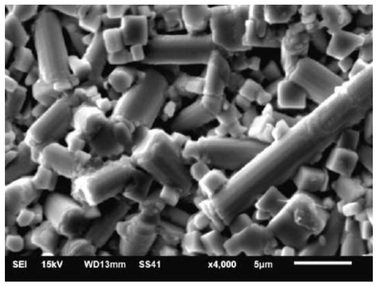

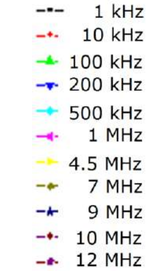

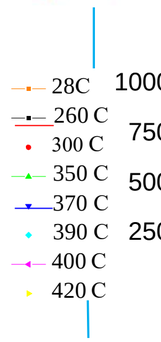

mKNN + TeO_2

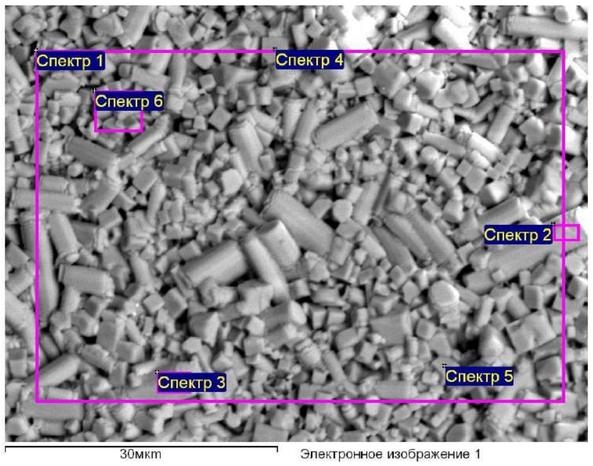

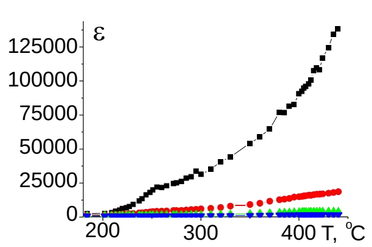

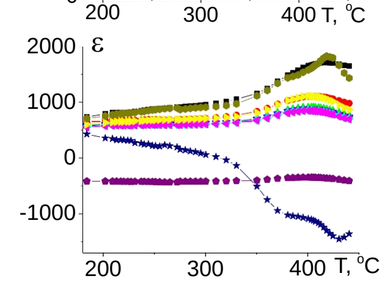

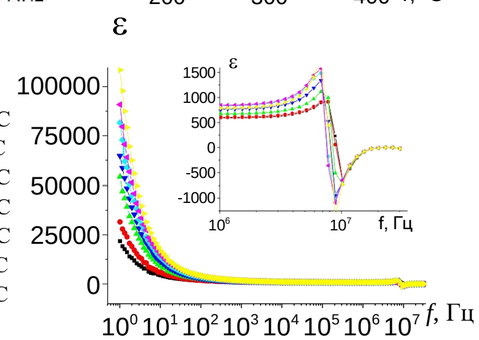

Surface images and element composition of the samples obtained by used a JEOL 6610 LV scanning electron microscope, by used an energy-dispersive microanalysis (EDM analysis system of Oxford INCA).

The inclusion of paratellurite in mKNN ceramics changes the shape and increases the grain size by an order of magnitude. Thus, if grains containing only mKNN material have a cubic shape, then the presence of tellurium leads to the formation of grains in the form of sufficiently long tubes (when the length is several times greater than the diameter) with a porous internal structure.

spectrum	O	Na	K	Ti	Sr	Nb	Te	Ta
spectrum 1	38.32	5.10	5.40	0.74	1.10	46.50	1.06	1.80
spectrum 2	38.22	2.58	5.48	0.63	1.71	48.61	0.72	2.06
spectrum 3	39.76	4.85	5.95	0.59	0.56	45.47	1.31	1.13
spectrum 4	42.21	9.11	3.58	0.47	1.23	41.98		1.42
spectrum5	46.39	2.04	5.81	0.57	0.55	41.35	1.71	1.59
spectrum 6	40.36	7.93	4.13		1.36	43.94		2.01

The dispersion of the dielectric permittivity was measured by the LCR method using the Frequency Response Analyzers PSM1735 with Impedance Analysis Interface (Newtons4th Ltd)

Temperature studies carried out in the frequency range from 1 Hz to 15 MHz have shown that the addition of TeO_2 to the mKNN composition leads to the disappearance of the additional maximum observed for mKNN on the temperature dependence of the permittivity in the region of 220–250°C. This maximum corresponds to a structural phase transition in KNN ceramics. On the temperature dependences of the permittivity, anomalies at a temperature close to the Curie temperature attract attention - a minimum with negative values of the permittivity at frequencies above 9 MHz. The meaning of the negative permittivity in this situation is the presence of resonant processes in the dielectric response.

The presence of resonance processes in the high-frequency region at high temperatures is confirmed by studies of **the frequency dependences of the permittivity**. With the introduction of paratellurite, a distinct peak appears in the modified mKNN ceramics, the shape of which is similar to that of the piezoelectric resonance–antiresonance. In the absence of a paratellurite impurity in the mKNN ceramic sample, the resonant component of the peak is absent, and only a weak antiresonance minimum takes place. The presence of a minimum with a flat maximum means the existence of a relaxation dispersion in the material, while the presence of a maximum and a minimum simultaneously indicate about resonant dispersion.

Thus, the introduction of paratellurite into ceramics mKNN changes both the shape and increases the grain size by an order of magnitude and the type of permittivity dispersion, i.e., the behavior of the material in an AC electric field.